

# Simulating local Green Gas feed-in through constant gas flow control

Jeroen van Es

30 June 2016



**Utrecht University**

## **Colophon**

**Title:**

*Simulating local Green Gas feed-in through constant gas flow control  
Internship report*

**Institution:**

*Utrecht University  
GEO4-2520 Internship Energy Science*

**Host organisation:**

*Kiwa Technology B.V.*

**Author:** *Jeroen van Es*

**Student number:** *5573912*

**E-mail address:** *jeroenvanes@live.nl*

**Supervisor Utrecht University:**

*Dr. Evert Nieuwlaar*

**Supervisor Kiwa Technology B.V.**

*Ir. Hans de Laat*

## Executive summary

Green Gas is an energy carrier that is increasingly produced in the Netherlands and is used to replace a share of the natural gas in the gas grid as part of the energy transition. It is fed into local gas grids, which forms a challenge for distribution system operators. In order to test how a distribution system operator should act when multiple Green Gas feeders are active in one gas grid, Stedin has developed a constant flow controller for natural gas to simulate a local Green Gas producer. Kiwa is setting up a demonstration in which the realised feed-in capacity of Green Gas will be allocated over the constant flow controller and one existing Green Gas producer.

Earlier tests have shown the potential of realising more capacity for Green Gas in local gas grids during summer. However, it had also become clear that the current flow control was not stable when sudden pressure variations occurred. Therefore, in this research, a new control algorithm for the constant flow rate controller has been designed, which assures that the flow of gas remains equal to the chosen set point under all circumstances.

This algorithm calculates the flow through the system by applying the geometry of the ball valve in the system. The algorithm recognises the set point, the pressure in the grid, the pressure difference across the valve and the gas temperature as input variables. Other system parameters, such as internal pressure loss, are shown to be negligible.

In order to keep the flow through the valve close to the set point, the valve will need to be continuously adjusted based on the input signals. The new control continuously calculates the difference between the set point flow and the measured flow, as it tries to minimise the difference between both by changing the position of the valve.

The new control concept has been tested in both a model and in a field test, where it is able to sustain a constant flow within 10% of the set point. Furthermore, it shows to provide better results in responding quickly to changing circumstances and, unlike the old control, does so without skipping the set point. All that rests for the new algorithm is to prove itself during the demonstration project.

## Table of contents

1	Introduction .....	1
1.1	Background.....	1
1.2	Problem definition.....	1
1.3	Research aim .....	2
1.4	Research question .....	2
1.5	Social relevance .....	2
1.6	Project boundaries .....	2
1.7	Report structure.....	3
2	Theoretical framework.....	4
2.1	Valve characteristics .....	4
2.2	Input signals.....	8
2.3	System constraints .....	11
3	Methodology.....	15
3.1	Constant flow control .....	15
3.2	Simulation of the control concept.....	16
3.3	Field test.....	25
4	Results .....	26
4.1	Dead valve stroke .....	26
4.2	Characteristic of the valve .....	26
4.3	Sensitivity of control concept .....	26
4.4	Operation of the valve .....	27
4.5	Valve behaviour in critical situations.....	29
4.6	Field test.....	31
5	Discussion .....	32
5.1	Methodology .....	32
5.2	General simplifications .....	32
5.3	Modelled environment .....	33
6	Conclusion .....	35
6.1	Recommendations .....	35
7	References .....	36
	Appendix.....	I
A.	Friction coefficient characteristics .....	I
B.	SG3 system .....	II
C.	Dynamic viscosity .....	III
D.	Pressure loss in the system .....	IV
E.	Critical pressure ratio .....	VIII
F.	Supporting graphs .....	XI

## List of figures

Figure 2.1.1 - working of a ball valve .....	4
Figure 2.1.2 - operation of ball valve .....	4
Figure 2.1.3 - dead valve stroke.....	5
Figure 2.1.4 - opening of the ball valve.....	6
Figure 2.1.5 - calculation of x .....	7
Figure 2.1.6 - sector area .....	8
Figure 2.1.7 - area triangle .....	8
Figure 2.2.1 - ball valve friction coefficient characteristic curve.....	10
Figure 2.3.1 - schematic overview of the SG3 system.....	11
Figure 3.2.1 - model of gas grid .....	18
Figure 3.2.2 - model of gas receiving station delivery.....	18
Figure 3.2.3 - model of Green Gas feed-in .....	19
Figure 3.2.4 - model of gas consumption.....	19
Figure 3.2.5 - model of pressure change.....	20
Figure 3.2.6 - model of pressure in gas grid .....	20
Figure 3.2.7 - model of control concept.....	20
Figure 3.2.8 - model of relative delta set point .....	21
Figure 3.2.9 - model of delta set point setting.....	21
Figure 3.2.10 - model of pressure difference .....	22
Figure 3.2.11 - model of pressure difference setting.....	22
Figure 3.2.12 - model of control setting.....	22
Figure 3.2.13 - model of valve position factor.....	23
Figure 3.2.14 - model of sign delta set point.....	23
Figure 3.2.15 - model of valve position change .....	23
Figure 3.2.16 - model of valve position.....	24
Figure 3.2.17 - model of valve flow.....	24
Figure 3.2.18 - model of calculated flow.....	25
Figure 3.2.19 - model of measured flow .....	25
Figure 4.2.1 - ball valve flow characteristic.....	26
Figure 4.3.1 - sensitivity analysis of input signals on the flow through the valve .....	27
Figure 4.4.1 - pressure in the test grid.....	27
Figure 4.4.2 - pressure difference across the valve.....	28
Figure 4.4.3 - position of the valve .....	28
Figure 4.4.4 - measured flow through the valve.....	29
Figure 4.5.1 - pressure in the gas grid on 3-9-2013/4-9-2013 .....	29
Figure 4.5.2 - pressure difference across the valve on 3-9-2013/4-9-2013 .....	30
Figure 4.5.3 - position of the valve on 3-9-2013/4-9-2013 .....	30
Figure 4.5.4 - Measured flow through the valve on 3-9-2013/4-9-2013 .....	31
Figure 4.6.1 - results of field test.....	31
Figure 5.1.1 - calculated flow versus the measured flow through the valve for the 2013 field test.....	32
Figure 5.1.2 - data points grouped on pressure difference .....	32
Figure A.1 - friction coefficient characteristic curve of a slider, lower line (Kast & Nirschl, 2013) .....	I
Figure B.1 - the current SG3 system at gas receiving station Baarn.....	II
Figure C.1 - Dynamic viscosity $\mu_{t,1}$ for gases as a function of temperature $t$ and Molar mass $M$ with a correction factor for the presence of $N_2$ , $CO_2$ and $H_2S$ inserted (Geerssen, 1988) .....	III
Figure C.2 - Viscosity ratio $m$ as a function of reduced pressure $p_r$ and reduced temperature $T_r$ (Geerssen, 1988) .....	III
Figure D.1 - gradual enlargement in pipes .....	V
Figure D.2 - gradual contraction in pipes .....	VI
Figure D.3 - Friction coefficient $\zeta$ for flow into a tee with a blind flange on the one branch (Kast & Nirschl, 2013) .....	VII
Figure D.4 - characteristic for a butterfly valve (Kast & Nirschl, 2013).....	VII
Figure E.1 - $\Delta c_p^0$ as a function of reduced pressure $p_r$ and reduced temperature $T_r$ (Geerssen, 1988) .....	X
Figure E.2 - $\Delta c_p'$ as a function of reduced pressure $p_r$ and reduced temperature $T_r$ (Geerssen, 1988) .....	X
Figure F.1 - gas receiving station delivery, the peak at $0,7 \times 10^6$ is due to the modelled gas receiving station correcting for missing data in the used dataset.....	XI
Figure F.2 - gas consumption in the model, peaks are due to noise reduction.....	XI

# List of tables

- Table 2.2.1 - symbols used in equation ( 20 ) ..... 10
- Table 2.3.1 - pressure loss in system ..... 13
- Table 3.1.1 - control routines ..... 15
- Table 3.1.2 - incremental adjustment..... 15
- Table 3.2.1 - Legend of model blocks..... 17
- Table E.1 - Constants for the compressibility factor (Geerssen, 1988) ..... IX
- Table E.2 -  $c_p^0$  of Dutch natural gas..... X



# 1 Introduction

In order to increase their share of renewable energy, the Netherlands has formulated a target for synthetic natural gas from biomass to be fed into the gas distribution grid of 202 ktoe per year for 2015 and 582 ktoe per year for 2020 (Beurskens et al., 2011). This is interpreted as a combined target for the entire range of biogases from biomass (SNG and bio-methane) upgraded to the standard of natural gas in the public Dutch network. In this research, all of these biogases shall be referred to as Green Gas, regardless of biomass source. It is expected that Green Gas will be increasingly produced and fed-in locally, which forms a challenge for distribution system operators, because gas grids have not been designed for local feed-in of gas.

After receiving multiple appeals for the feeding-in of Green Gas, distribution system operator Stedin has started a pilot project to look into the opportunities of Smart Green Gas Grids (SG3). As distribution system operator, it is the responsibility of Stedin to allocate the feed-in capacity over the active Green Gas feeders in a grid.

Because there is no practical experience with having multiple Green Gas feeders active in one gas grid, Stedin has developed a constant flow control for natural gas to simulate a local Green Gas producer. By keeping the gas flow rate constant, the system best resembles a Green Gas producer.

Through feeding Green Gas at a constant flow into the grid, the pressure in the gas grid will vary, since consumption fluctuates daily. This allows for input of Green Gas into the grid at moments with low gas consumption. Kiwa is supporting Stedin in setting up a demonstration in which the realised feed-in capacity of Green Gas will be allocated over multiple Green Gas producers.

## 1.1 Background

This research will follow up on SG3 projects executed in 2012/2013. In 2013, a demonstration project in the gas grid of Bunschoten and Eemnes was performed by applying constant flow regulation in order to create maximal pressure variation in the gas grid. During a couple of weeks in the summer, additional capacity for feed-in of Green Gas was made available, through varying the pressure in the gas grid. This allowed for the storage of Green Gas in the gas grid during the night; the stored gas is consumed during the daily consumption peak. This test has shown that varying the pressure in a local gas grid is a cheap and reliable way of realising more capacity in the local gas grid during summer.

This current option for a smart gas grid is restricted to a manual change in minimal absolute gas grid pressure from 9 bar to 5,5 bar during spring and vice-versa after roughly six months. An absolute pressure in the gas grid of at least 5,5 bar is maintained by the gas receiving stations operated by Gasunie.

This research will make use of the same gas grid as the 2013 demonstration project. The test grid is the first artificially created site in the Netherlands where more than one local gas feeder is active.

## 1.2 Problem definition

During the 2013 demonstration, it became clear that the current flow control is not stable when sudden pressure variations occur. Therefore, the control of the SG3 system should be modified in such a way that (1) in all circumstances the set point gas flow through the SG3 system is stable and (2) the system responds quickly when conditions change.

The general idea is that these problems can be solved by developing a new algorithm for multivariable control in the constant flow controller. The development of a new algorithm has been chosen as a solution over developing a new SG3 system because of the high costs of designing such a system.



### 1.3 Research aim

A new demonstration of dynamic gas grid management in 2016 requires multiple settings of a desired flow through the valve. This is referred to as 'set point flow rate' or 'set point', which will be set remotely and should be maintained without supervision. The dynamic behaviour of the present system is expected insufficiently stable for this task. Therefore, a new control algorithm for the constant flow rate controller is to be designed, which assures that the flow of gas remains equal to the chosen set point under all circumstances.

The SG3 system was developed to look into methods of prioritisation of local Green Gas feeders, so it should be designed to allow for experimenting with prioritisation. The new functionalities of the system are developed in respect to four capacity allocation strategies:

- Last-in-first-out (all of the capacity is allocated to the producer with the oldest rights)
- Share the pain (all producers get the same allocated capacity)
- Green Gas Doubling (find a balance between the buffer capacity and operational reliability)
- Outside temperature sensing (pressure in the grid will be based on the outside temperature)

The experiments itself will take place during the demonstration in the summer of 2016, which is beyond the scope of this research.

### 1.4 Research question

The following main research question has been determined:

*'How can it be assured that the flow of gas from the constant flow rate controller remains equal to the set point under all circumstances?'*

In order to answer this research question, the following sub-questions have to be answered first:

1. What is the characteristic of the valve in the constant flow controller?
2. What input signals should be used for the constant flow control?
3. What system constraints restrict dynamic behaviour of the constant flow control?
4. How can it be tested that the constant flow rate controller works under all circumstances?

### 1.5 Social relevance

This research will support the development of the technology of the SG3 system in sustaining a lower pressure in local gas grids in the summer months. This leads to an increase of maximal Green Gas storage capacity during summer, better accuracy of gas meters and less losses of gas through leakage. The reason that it only leads to an increase of Green Gas capacity in the summer, is that Green Gas capacity is not limited during other months, since consumption then is larger than Green Gas feed-in. Next to this, this project is part of the energy transition as it concerns replacing a share of the natural gas in the gas grids with sustainable Green Gas.

### 1.6 Project boundaries

Changes and additions to the gas-flow control are implemented into the control unit of the SG3 system by the company gAvilar. The actual demonstration is done by Kiwa in 2016 (weeks 31, 32 and 33) since the gas consumption during these weeks is small, but still large enough to be supplied by two biogas feeders. In build-up to the demonstration, several pressure reductions in the gas grid will be realised by Gasunie to check the condition of the test grid.

During the initial field tests a problem with feed-in of biogas was experienced due to the lower pressure in the gas grid. As a result, the minimal absolute pressure reached during this demonstration will be 6 bar instead of the 5,5 bar that has been realised in the 2013 field tests.

## 1.7 Report structure

In order to answer the research questions, a theoretical framework has been developed in chapter 2, in which the theory necessary to answer the research questions is described. In order to answer sub-question 1, the characteristics of the valve are estimated by applying the valve geometry defined in paragraph 2.1 to formulate a standard to calculate the exact area in the valve through which gas can flow through. Situational parameters, such as a dead valve stroke, are also taken into account.

The theory necessary to answer sub-question 2 is described in paragraph 2.2, where the theory defined in paragraph 2.1.2 is applied to formulate a general formula to calculate the flow of gas through the valve. The variables in this formula are tested on its sensitivity to the operation of the control concept so the most important input signals can be defined.

In order to answer sub-question 3, the theory necessary to observe whether system constraints influence the behaviour of the constant flow control is described in paragraph 2.3.

The theory in chapter 2 is used to develop the control concept described in chapter 3. The control concept is tested in both a model as well as in a field test; this is described in paragraphs . In order to test its behaviour under a wide range of circumstances, the control concept is modelled in Simulink, which is a graphical programming environment within MATLAB. The final settings of the control concept are determined through field testing.

The results are obtained from testing the constant flow control in the model. These results are discussed in the discussion, after which the conclusion is given which provides the answer to the research question. Thereafter, some recommendations are given.

## 2 Theoretical framework

### 2.1 Valve characteristics

In order to determine the valve characteristics, the geometry and functioning of the valve need to be clear. The particular type of valve used in the SG3 system is a ball valve; the basic working of a ball valve is shown in Figure 2.1.1.

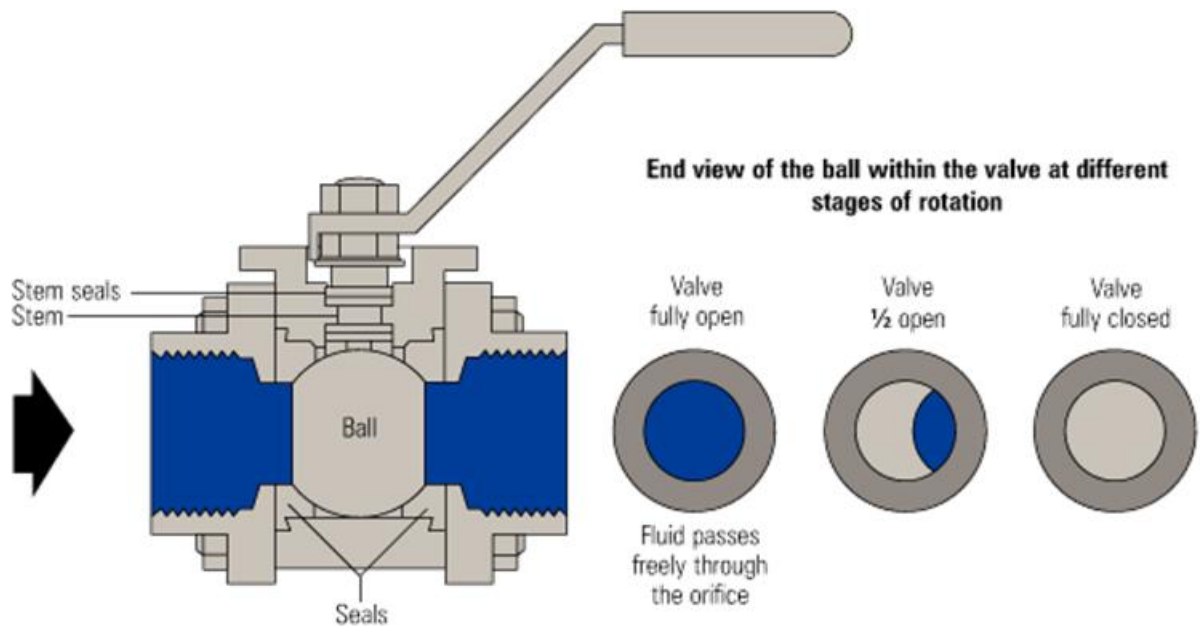


Figure 2.1.1 - working of a ball valve<sup>1</sup>

The valve is operated by the handle and can be operated over 90 degrees, where the valve is fully closed at 0° and fully open at 90°, as shown in Figure 2.1.2.

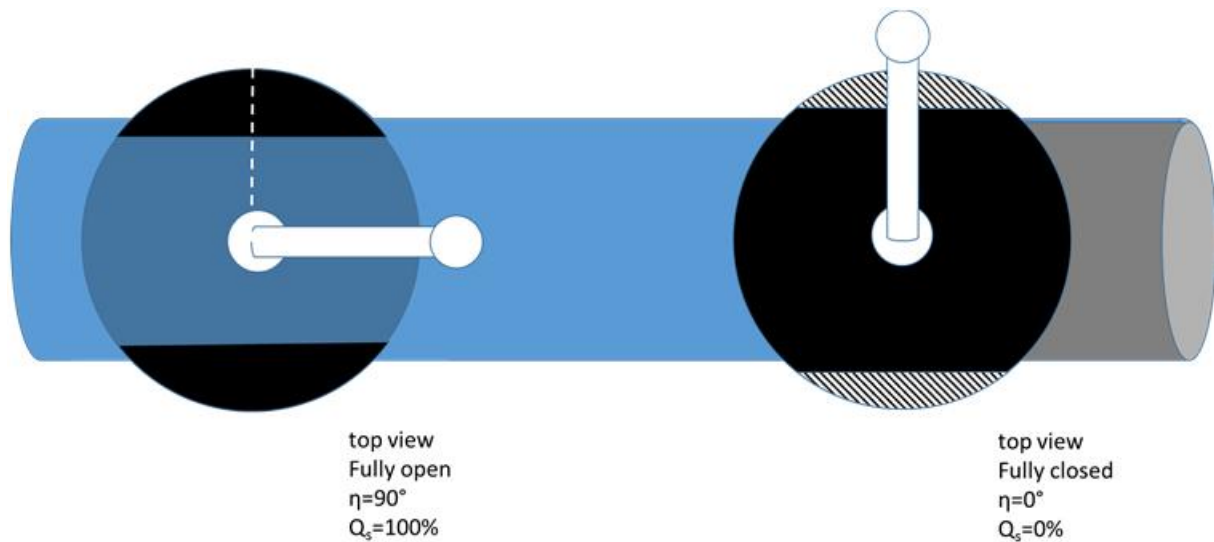


Figure 2.1.2 - operation of ball valve

<sup>1</sup> [http://www.spiraxsarco.com/Resources/Pages/Steam-Engineering-Tutorials/Images/12/2/fig\\_12\\_2\\_1.gif](http://www.spiraxsarco.com/Resources/Pages/Steam-Engineering-Tutorials/Images/12/2/fig_12_2_1.gif)

In order to precisely calculate the flow of gas through the valve, the distribution of flow needs to be determined as a function of the position of the valve. It is assumed that all geometric shapes in the ball valve are perfect. The variables in this distribution function of the flow through the ball valve ( $Q_s$ ) are the position ( $\eta$ ) of the valve, the diameter of the opening in the ball ( $d_o$ ), the diameter of the pipe ( $d_p$ ) and the relative angle of the valve ( $h$ ).

### 2.1.1 Dead valve stroke

In the 2013 demonstration project, it was found that the valve does not open from  $0^\circ$  on because at small positions there was no flow through the valve. The size of the dead valve stroke is estimated using data from the 2013 demonstration project and will be verified during field tests on the current SG3 system. Dead valve stroke  $\eta_d$  is defined as the position of the valve at which no gas flows through the valve at all positions smaller than  $\eta_d$ , while gas flow through the valve does occur for all positions larger than  $\eta_d$ .

Free valve stroke  $\eta_f$  applies at the fully opened position, where the free valve stroke is the position at which no increase in gas flow occurs for all positions larger than  $\eta_f$ . It is assumed that the pipe is symmetrical, and that therefore  $\eta_f$  can be expressed as:

$$\eta_f = 90 - \eta_d \quad (1)$$

Once the dead and free valve stroke have been acquired, they have to be integrated into the calculation of the angle of the valve. Here the distinction is made between the absolute position of the valve  $\eta$  and the relative operating angle of the valve  $h$ . This is shown in Figure 2.1.3.

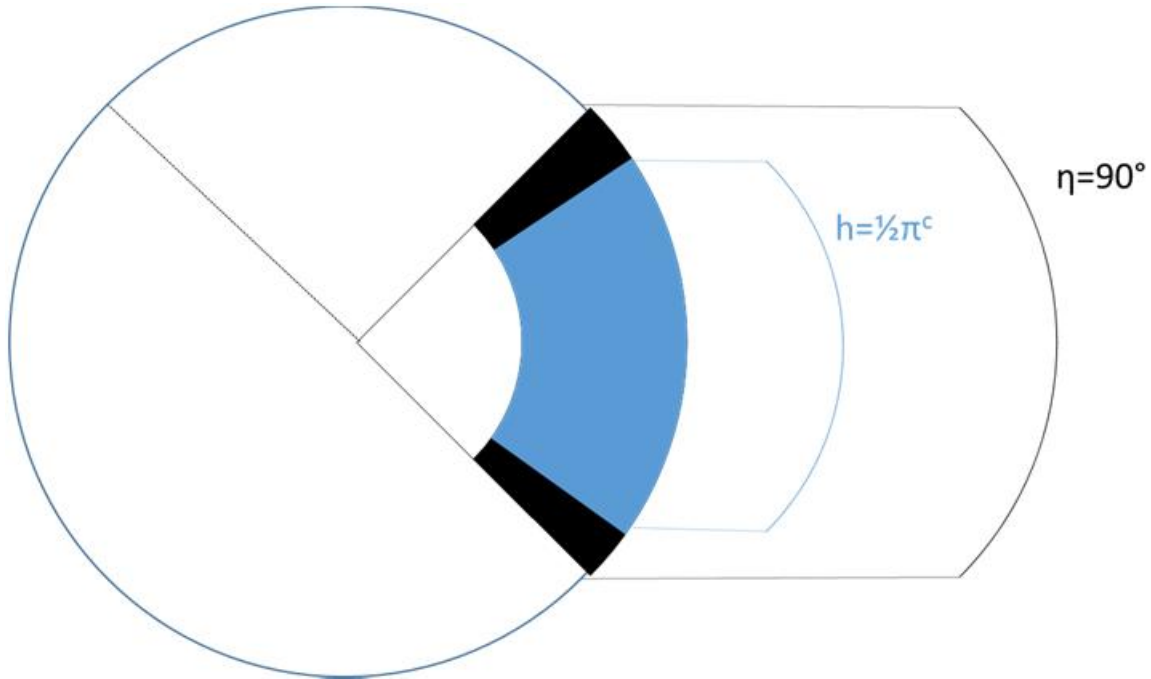


Figure 2.1.3 - dead valve stroke

Now, the gas flow through the ball valve can be calculated for each relative angle  $h$ , where  $h$  in radians is expressed as:

$$h = \frac{90 * (\eta - \eta_d)}{90 - 2 * \eta_d} * \frac{\pi}{180} \quad (2)$$

for  $\eta_d < \eta < \eta_f$ . For  $\eta < \eta_d$ ,  $h = 0$  and for  $\eta > \eta_f$ ,  $h = \frac{1}{2}\pi$ , with  $\eta$ ,  $\eta_d$  and  $\eta_f$  in degrees.

### 2.1.2 Gas flow through valve

When the pipe and ball valve opening are equal ( $d_p=d_o$ ), the flow of gas is calculated by first calculating the area through which gas can flow. In Figure 2.1.4 is shown that an ellipse-shaped area is created by overlap from the pipe and the opening of the valve at certain relative angles  $h$ . This has been simplified into a two-dimensional picture. For each relative angle  $h$ , minor axis  $x$  of the ellipse (the shortest diameter) is calculated, as shown in Figure 2.1.5, by:

$$x = \frac{1}{2} + \frac{1}{2} * \tan \left( h - \frac{1}{4}\pi \right) \quad (3)$$

For an exemplar relative angle  $h$  of  $\frac{1}{6}\pi$ ,  $x$  is 0,366.

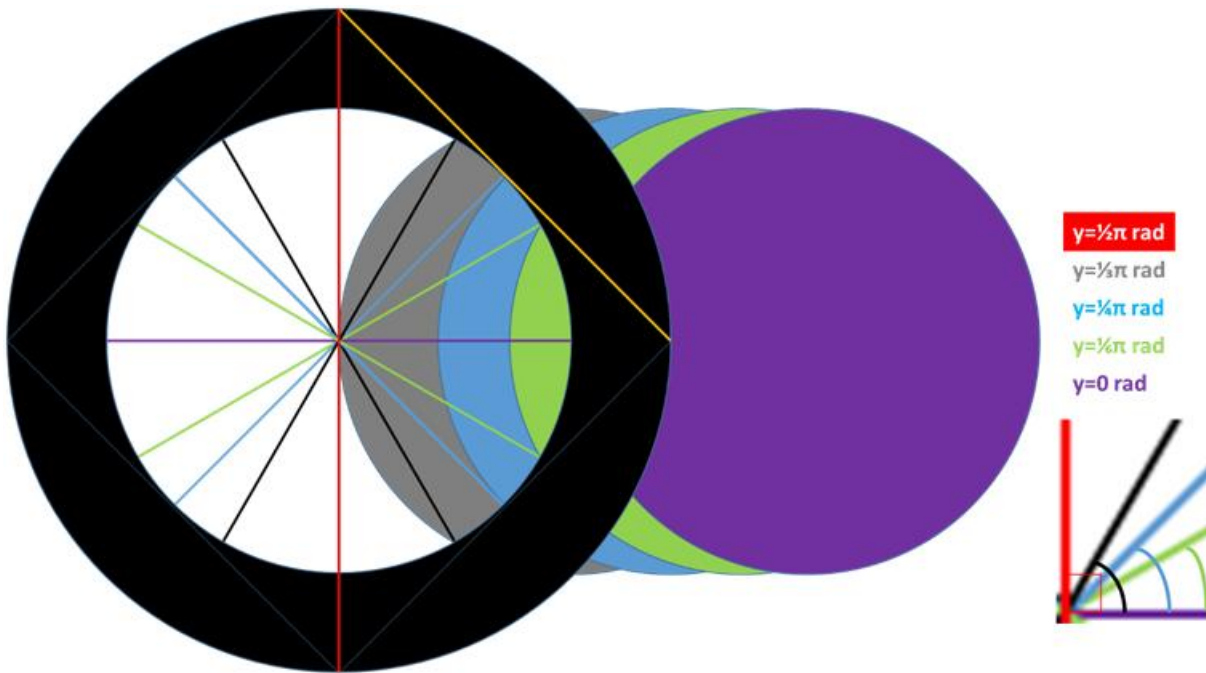


Figure 2.1.4 - opening of the ball valve

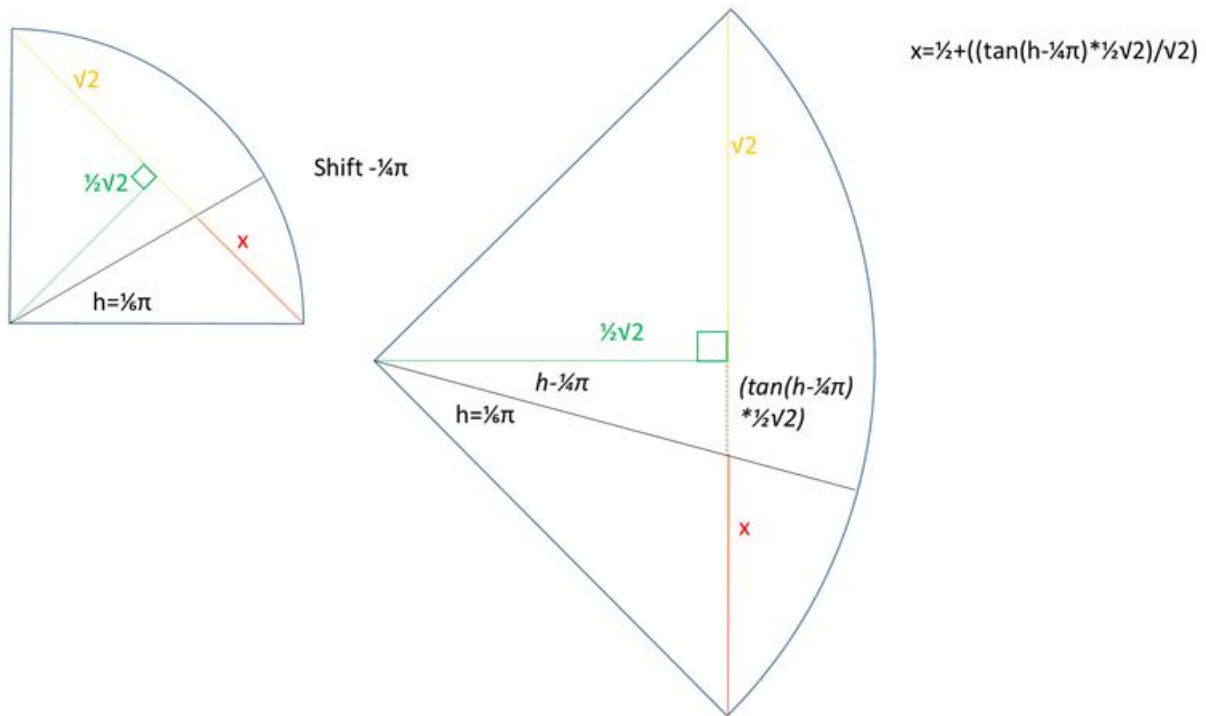


Figure 2.1.5 - calculation of  $x$

Using minor axis  $x$ , the angle  $y$  at which the opening of the pipe intersects with the opening of the valve can be determined through:

$$y = \cos^{-1}(1 - x) \quad (4)$$

which in case of relative angle  $h$  of  $\frac{1}{6}\pi$  and  $x$  of 0,366 gives  $y$  of 0,884 rad.

In Figure 2.1.4, five angles  $y$  are shown (0 rad,  $\frac{1}{6}\pi$  rad,  $\frac{1}{4}\pi$  rad,  $\frac{1}{3}\pi$  rad and  $\frac{1}{2}\pi$  rad). When the diameter of the pipe is equal to that of the ball valve opening ( $d_o = d_p$ ), the area of any ellipse in Figure 2.1.4 is calculated by first determining the sector area  $A_s$  between the corresponding lines:

$$A_s = \frac{1}{4}y \times d_o^2 \quad (5)$$

Sector area  $A_s$  in Figure 2.1.6 for  $h$  of  $\frac{1}{6}\pi$  and  $d_o$  of 50 mm is 552 mm<sup>2</sup>.

In order to obtain the area of the green ellipse in Figure 2.1.4, the area of the yellow triangle  $A_t$  in Figure 2.1.7 needs to be calculated using the following formula:

$$A_t = \frac{1}{8}d_o^2 \times \sin(2y) \quad (6)$$

For  $h$  of  $\frac{1}{6}\pi$  and  $d_o$  of 50 mm, the area of triangle  $A_t$  is 306 mm<sup>2</sup>.

The area of the green ellipse  $A_e$  in Figure 2.1.4 is then calculated with:

$$A_e = 2 \times (A_s - A_t) \quad (7)$$

This yields an area for the gas to flow through of 492 mm<sup>2</sup> at  $h$  of  $\frac{1}{6}\pi$  and  $d_o$  of 50 mm. This area  $A_e$  is equal to 25,07% of the total valve capacity  $A_0$ , according to:

$$\zeta_h = \frac{A_e}{A_0} \quad (8)$$

where  $c_h$  is the percentile opening of the valve at relative angle  $h$  and total valve capacity  $A_0$  is calculated through:

$$A_0 = \frac{1}{4}\pi d_o^2 \quad (9)$$

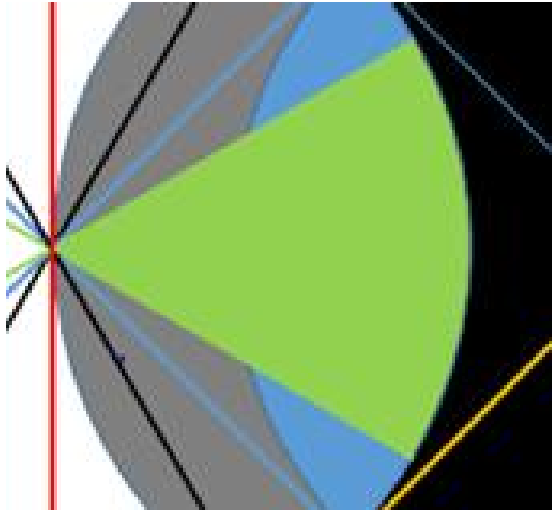


Figure 2.1.6 - sector area

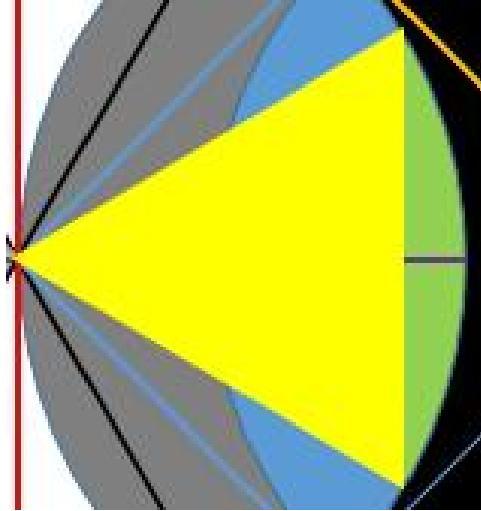


Figure 2.1.7 - area triangle

The relative opening of the ball valve is found to be calculated through:

$$c_h = \frac{2 \cos^{-1} \left( \frac{1}{2} - \frac{1}{2} \tan \left( h - \frac{1}{4} \pi \right) \right) - \sin \left( 2 \cos^{-1} \left( \frac{1}{2} - \frac{1}{2} \tan \left( h - \frac{1}{4} \pi \right) \right) \right)}{\pi} \quad (10)$$

which is based on equations ( 3 ) through ( 9 ) with relative angle  $h$  as the only variable.

## 2.2 Input signals

The algorithm for the control valve should determine at what angle the valve needs to be operated in order to allow a stable set point flow. The method of checking the area of the opening in the cross-section of the ball valve at a certain angle  $h$  has already been determined in chapter 4.2. This will be used in reverse by determining an angle  $h$  to realise the percentile opening to allow a set point flow through the valve. This opening ( $c_h$ ) is calculated through dividing set point flow rate  $Q_s$  by the free (of restriction) flow rate  $Q_f$  in the system:

$$c_h = \frac{Q_s}{Q_f} \quad (11)$$

Set point  $Q_{sn}$  has to be converted to  $m^3/s$ , as it is set in normal cubic meters per hour. Normal cubic meters describe the volume of gas under normal pressure (1,01325 bar) and temperature (273,15 K). The set point is converted through:

$$Q_s = \frac{Q_{sn}}{3600} * V_o \quad (12)$$

where  $Q_{sn}$  is the set point in normal cubic meters ( $Nm^3/h$ ) and  $V_o$  is the operational volume of one normal cubic meter of gas. This is obtained through rewriting the combined gas law:

$$V_o = \frac{T_o p_n V_n}{p_o T_n} \quad (13)$$

where the volume in m<sup>3</sup> of 1 normal cubic meter of gas (V<sub>o</sub>) is obtained from the absolute pressure of the gas p<sub>o</sub> in bar and absolute temperature T<sub>o</sub> in kelvin of the gas in the grid, while taking the normal temperature T<sub>n</sub> of 273,15 K, normal pressure p<sub>n</sub> of 1,01325 bar and normal volume V<sub>n</sub> of 1 m<sup>3</sup>.

### 2.2.1 Free volumetric flow in system

Free flow rate Q<sub>f</sub> in m<sup>3</sup>/s is calculated by:

$$Q_f = A_p \times v_f \quad (14)$$

where cross-sectional area of the pipe A<sub>p</sub> in m<sup>2</sup> is obtained through:

$$A_p = \frac{1}{4} \pi d_p^2 \quad (15)$$

with d<sub>p</sub> being the diameter of the pipe in meters. Flow velocity v<sub>f</sub> in m/s is defined as:

$$v_f = \sqrt{\frac{2\Delta p}{\zeta \rho}} \quad (16)$$

where ζ is the dimensionless friction coefficient (further explained in chapter 2.2.3), ρ is the density in kg/m<sup>3</sup> and Δp is the pressure difference in pascal, defined as:

$$\Delta p = p_A - p_o \quad (17)$$

where p<sub>A</sub> is the absolute pressure at the beginning of the pipe (the grid of Amersfoort) and p<sub>o</sub> is the absolute pressure at the end of the pipe (the test grid). All pressures are in pascal.

### 2.2.2 Density

Density ρ in kg/m<sup>3</sup> is defined as:

$$\rho = \frac{p_o M}{z R_a T_o} \quad (18)$$

where p<sub>o</sub> is the absolute pressure of the gas in the grid in Pa, M is the molar mass of Dutch natural gas (1,8637\*10<sup>-2</sup> kg/mol), z is the dimensionless compressibility factor of Dutch natural gas (0,9977), R<sub>a</sub> is the universal gas constant (8,31441 J/(mol\*K)) and T<sub>o</sub> is the absolute temperature of the gas in the grid in kelvin (Geerssen, 1988).

### 2.2.3 Friction coefficient

Dimensionless friction coefficient ζ resembles the friction that the gas is subject to when passing through the ball valve. The friction coefficient is a function of the relative opening of the valve ζ<sub>h</sub>. It is assumed to behave as a slider in a square pipe, with the adjustment that the opening is not measured in one-dimension (which is possible in a square pipe), but in two dimensions. This is done by measuring the cross-sectional area relative to the total cross-sectional area in the valve (ζ<sub>h</sub>). In Figure 2.2.1, the friction coefficient characteristic curve for a slider is shown, which has been deduced from Appendix A (Kast & Nirschl, 2013). Two trend lines are fitted to this curve (power and exponential). On the basis of these trend lines, another relation is developed, for which the curve is shown in orange, which is:

$$\zeta = -1,2 + 1,4 * \zeta_h^{-2} \quad (19)$$



Note that multiple equations with relative opening of the ball valve  $\zeta_h$  as variable are used throughout this research. In this case, equation ( 8 ) is used, since the other equations are dependent on the value of the friction coefficient.

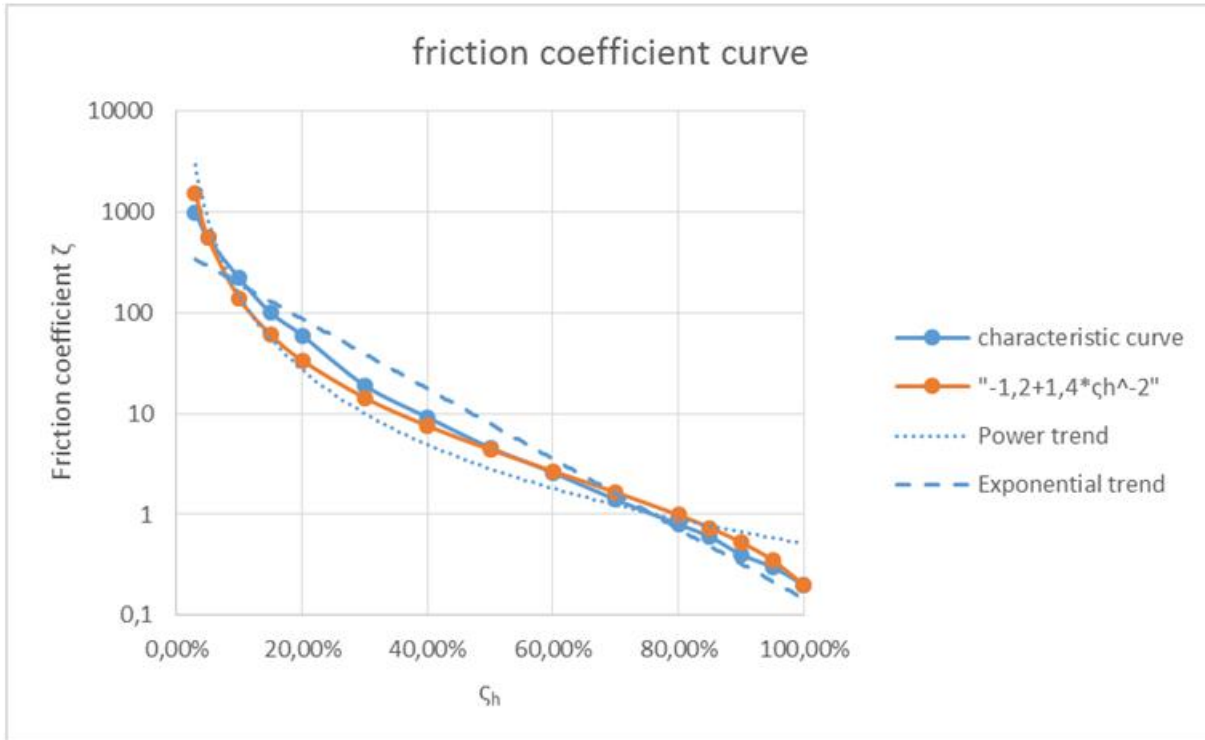


Figure 2.2.1 - ball valve friction coefficient characteristic curve

#### 2.2.4 Flow through valve

The method of calculating the flow through the valve has been determined based on equations ( 11 ) through ( 19 ), with the symbols listed in Table 2.2.1:

$$\zeta_h = \frac{Q_{sn} * T_0 * p_n * V_n * \sqrt{p_0 * M * (-1,2 + 1,4 * \zeta_h^{-2})}}{900\pi * T_n * p_0 * d_p^2 * \sqrt{2 * \Delta p * z * R_a * T_0}} \quad (20)$$

Equation ( 20 ) is solved iteratively for  $\zeta_h$ , which is thereafter used in equation ( 10 ) to calculate relative angle h.

Table 2.2.1 - symbols used in equation ( 20 )

Input signals			Constants			
$Q_{sn}$	Set point	Nm <sup>3</sup> /h	$p_n$	Normal pressure	1,01325	bar
$T_0$	Temperature	K	$V_n$	Normal volume	1	m <sup>3</sup>
$p_0$	Pressure in grid	bar	$M$	Molar mass	1,8637*10 <sup>-2</sup>	kg/mol
$\Delta p$	Pressure difference	bar	$T_n$	Normal temperature	273,15	K
			$d_p$	Pipe diameter	0,05	m
			$z$	Compressibility factor	0,9977	-
			$R_a$	Universal gas constant	8,31441	J/(mol*K)

### 2.3 System constraints

In this paragraph, the constraints of this specific system will be discussed. A schematic overview of the system is shown in Figure 2.3.1, in which all components of the SG3 system are shown that are involved in the flow of gas between the gas grid of Amersfoort and the test grid of Bunschoten Eemnes. The gas goes above and below ground at the butterfly valves in segment 1. Gas flows from the high pressure side on the right (gas grid Amersfoort) to the low pressure side on the left (gas grid Bunschoten-Eemnes). When the gas pressure in the gas grid of Bunschoten-Eemnes is higher than that of Amersfoort, the gas flows through a non-return valve from segment 11 to segment 2 back to Amersfoort. This gas flow can be distinguished in Figure B.1 in Appendix B, but is not accounted for in this research.

For each numbered segment, the pressure loss due to friction is calculated. Segments that have the same number and colour have the same specifications. The gas meter (segment 5) is assumed to cause no pressure loss, because it is designed to operate at a very low resistance. The pressure loss in the ball valve (segment 9) is calculated in chapter 2.2.3. For the straight segment of pipe is assumed that it is a welded steel pipe with roughness factor of 0,1 mm and for the non-straight segments of pipe is assumed that these are cast-iron segments with roughness factor of 0,5 mm.

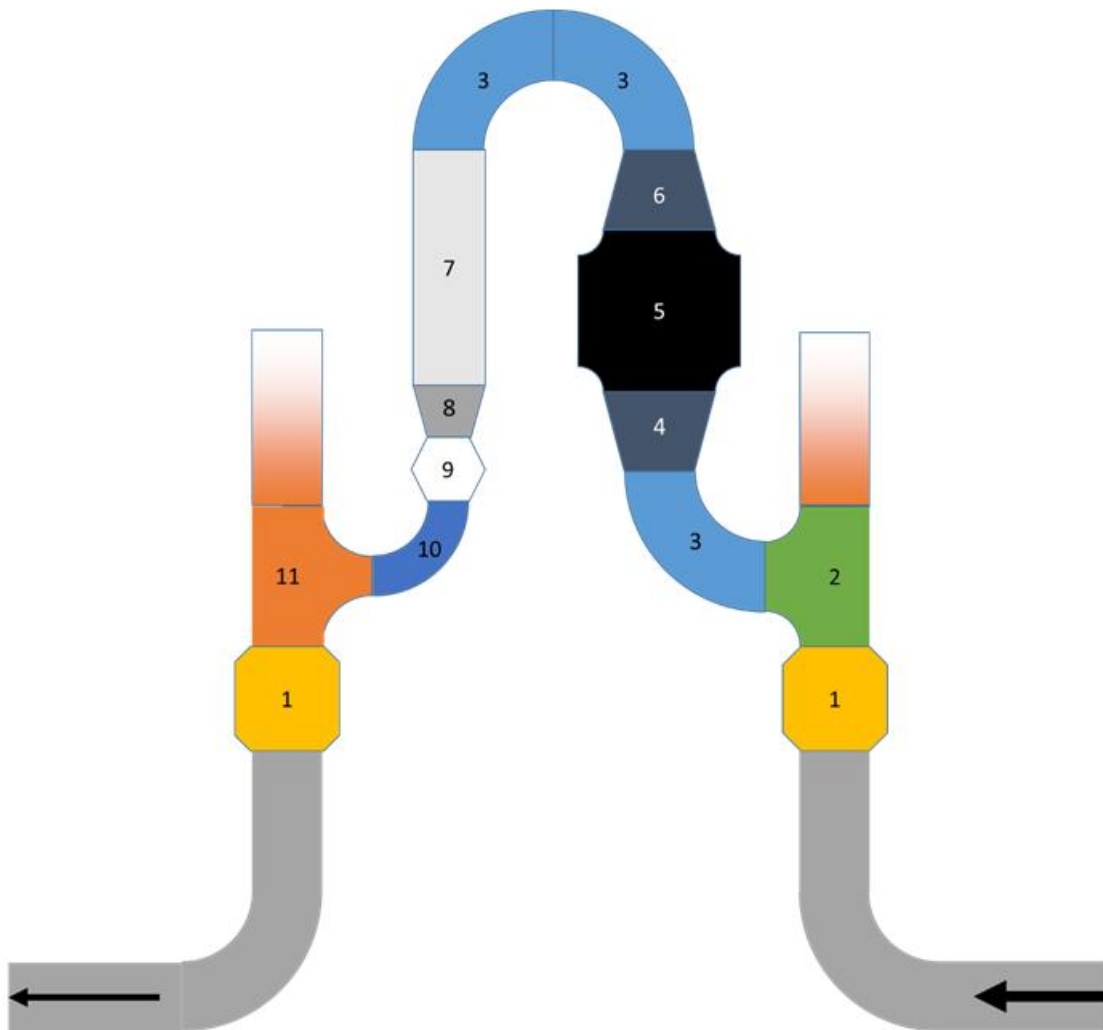


Figure 2.3.1 - schematic overview of the SG3 system

### 2.3.1 Reynolds number

The first step in determining the pressure loss per segment in the system is calculating the dimensionless Reynolds number for each segment flow through:

$$Re = \frac{v_a * d_a}{\nu} \quad (21)$$

where  $v_a$  is the average flow velocity in m/s,  $d_a$  is the average diameter of the pipe in meters and  $\nu$  is the kinematic viscosity in  $m^2/s$ . Average flow velocity  $v_a$  is obtained through rewriting equation (14) into:

$$v_a = \frac{Q_f}{A_a} \quad (22)$$

where average cross-sectional area  $A_a$  in  $m^2$  is obtained through:

$$A_a = \frac{1}{4} \pi d_a^2 \quad (23)$$

with  $d_a$  being the average diameter of the pipe in meters, calculated through:

$$d_a = \frac{d_1 + d_2}{2} \quad (24)$$

where  $d_1$  is the diameter of the start of the segment in meters and  $d_2$  is the diameter at the end of the segment in meters.

### 2.3.2 Kinematic viscosity

The kinematic viscosity is calculated through:

$$\nu = \frac{\mu_{T,p}}{\rho} \quad (25)$$

where  $\rho$  is the density as calculated through equation (18) and  $\mu_{T,p}$  is the dynamic viscosity. In order to calculate the pressure loss in the system, the pressure of the gas is assumed to be constant at the highest possible pressure in the grid, which is 9,01325 bar, while the temperature is assumed to be constant at 283,15 K. The dynamic viscosity  $\mu_{T,p}$  consists of three parts (Katz et al., 1959):

$$\mu_{T,p} = m * \mu_{T,pn} + \mu_c \quad (26)$$

$\mu_{T,pn}$  and  $\mu_c$  are obtained from Figure C.1 in Appendix C, which shows that  $\mu_{T,pn}$  for gas at a temperature of 10 °C (283,15 K) is  $10 * 10^{-6}$  Pa\*s. Correction factor  $\mu_c$  of  $1,17 * 10^{-6}$  Pa\*s is applied to compensate for the presence of  $N_2$  and  $CO_2$  in the Dutch natural gas mixture.

In order to obtain viscosity ratio  $m$  from Figure C.2 in Appendix C, the reduced pressure and reduced temperature have to be calculated. The reduced pressure is calculated through:

$$p_r = \frac{p}{p_c} \quad (27)$$

with  $p$  as the absolute grid pressure of the gas in kPa and  $p_c$  as the (pseudo-) critical pressure, which for Dutch natural gas is 4460 kPa (Geerssen, 1988). The reduced pressure is found to be 0,202 for an absolute grid pressure of 9,1325 bar.

The reduced temperature is calculated through:

$$T_r = \frac{T}{T_c} \quad (28)$$

with T as the absolute temperature of the gas in kelvin and  $T_c$  as the (pseudo-) critical temperature, which for Dutch natural gas is 187,0 K (Geerssen 1988). The reduced temperature is found to be 1,514 for a grid temperature of 283,15 K.

Viscosity ratio  $m$  is found to be 1,02 for reduced pressure  $p_r$  of 0,202 and reduced temperature  $T_r$  of 1,514. This gives a dynamic viscosity of  $11,37 \cdot 10^{-6}$  Pa\*s through equation (26). At absolute grid pressure of 9,1325 bar and grid temperature of 283,15 K, equation (18) gives a density of  $7,15 \text{ kg/m}^3$ . This gives a kinematic viscosity of  $1,59 \cdot 10^{-6} \text{ m}^2/\text{s}$  through equation (25).

### 2.3.3 Pressure loss in system

Table 2.3.1 shows the relevant known data (diameter and length) for each pipe segment, as well as the calculated average flow velocity through the pipe segment and the Reynolds number. The friction coefficients for each pipe segment are obtained from Appendix D; the specific paragraph that contains the calculation method for the pipe segment is also shown in Table 2.3.1. The pressure loss caused by the pipe segment is also shown in Table 2.3.1; if multiple segments exist within the system that share the same characteristics, the amount of segments is shown in brackets in the first column, while the total pressure loss for that indexed segment is shown in brackets in the second column of Table 2.3.1. The pressure loss is calculated through:

$$\Delta p = \frac{1}{2} \zeta \rho v_a^2 \quad (29)$$

in which  $\rho$  is the density of the gas as calculated through equation (18),  $v_a$  is the average flow velocity in m/s and friction coefficient  $\zeta$  is obtained from the paragraph specified per pipe segment in Table 2.3.1.

Table 2.3.1 - pressure loss in system

Numbered segment (#)	Pressure loss (Pa)	$v_a$ (m/s)	Re *	$d_1$ (m)	$d_2$ (m)	l (m)	$\zeta$	Paragraph
1 (2)	120,0 (240,0)	14,49	7,29E+05	0,08	0,08	0,1	0,2	D6
2	862,6	14,49	7,29E+05	0,08	0,08	0,2	1,15	D5
3 (3)	156,7 (470,0)	14,49	7,29E+05	0,08	0,08	0,2	0,209	D2
4	12,3	11,45	6,48E+05	0,08	0,1	0,1	0,026	D3
5	X	9,27	5,83E+05	0,1	0,1			2.3
6	16,9	11,45	6,48E+05	0,1	0,08	0,1	0,04	D4
7	99,4	14,49	7,29E+05	0,08	0,08	0,5	0,133	D1
8	44,7	21,94	8,97E+05	0,08	0,05	0,1	0,04	D4
9	X	37,08	1,17E+06	0,05	0,05			2.2.3
10	1103,6	37,08	1,17E+06	0,05	0,05	0,1	0,225	D2
11	1462,9	21,94	8,97E+05	0,05	0,08	0,1	0,85	D5

\*All flows are turbulent, since  $Re > 4000$  and rough, since  $\epsilon > 1,0 \cdot 10^{-5}$ . Equation (41) is used for calculating the friction factor of flows through bends, despite that the Reynolds number for these segments is larger than  $1 \cdot 10^5$ . All bends are  $90^\circ$  bends. The distance between the bends is at all times larger than the diameter of the pipe.

The total pressure loss in the SG3 system is  $4,4 \cdot 10^{-2}$  bar at a high set point of  $2000 \text{ Nm}^3/\text{h}$ . Since this is lower than the acceptable pressure loss of 0,1 bar, the pressure loss of the system is negligible.

#### 2.3.4 Critical pressure ratio

The flow through the system can choke when the pressure ratio over the SG3 system is lower than the critical pressure ratio  $p^*$ . Therefore, the pressure ratio in the gas grid is compared to the critical pressure ratio of the gas. The pressure ratio in the gas grid with maximum absolute pressure of 9,0 bar and minimum absolute pressure of 6 bar is found to be 0,7. The critical pressure ratio is calculated through:

$$p^* = \left( \frac{2}{k+1} \right)^{\frac{k}{k-1}} \quad (30)$$

where  $k$  is the dimensionless heat capacity ratio, which is calculated through:

$$k = \frac{c_p}{c_v} \quad (31)$$

in which  $c_p$  is the specific isobaric heat capacity in J/(mol\*K) and  $c_v$  is the specific isochoric heat capacity in J/(mol\*K). The isobaric heat capacity is found to be 36,45 kJ/(kmol\*K) and the isochoric heat capacity is found to be 27,10 kJ/(kmol\*K) in Appendix E. This gives a dimensionless heat capacity factor of 1,345 according to equation ( 31 ). Through equation ( 30 ) is found that the critical pressure ratio is 0,538. Since the pressure ratio in the gas grid (0,7) is higher than the critical pressure ratio, the flow through the SG3 system does not choke.

### 3 Methodology

The focus in chapter 2 has been to develop an equation to calculate the flow through the valve in a way that best approaches the measured flow through the valve. However, in order to keep the measured flow through the valve close to the set point, the valve will need to be continuously adjusted based on the input signals. This is done through the new control algorithm, which controls the flow through the valve. It continuously calculates the difference between the set point flow and the measured flow, as it tries to minimise the difference between both by changing the position of the valve.

#### 3.1 Constant flow control

By means of the relative difference between the set point  $Q_{sn}$  and the measured flow  $Q_m$ , the change in valve position is calculated. This relative delta set point is calculated through:

$$\delta_{sp} = \frac{(Q_{sn} - Q_m)}{Q_{sn}} \quad (32)$$

Every 20 seconds, the flow through the valve is communicated by the gas meter, after which the control determines an action. First,  $\delta_{sp}$  is calculated through equation (32), after which is determined with what control routine this corresponds. This is determined by looking up in what column in Table 3.1.1  $\delta_{sp}$  is located. This determines whether the control routine is either 'crude', 'normal' or 'fine', while it is also possible that no control action is necessary.

When a control routine is chosen (crude, normal or fine), the control routine that corresponds to the pressure difference is looked up in Table 3.1.1. Out of these two control routines (one for  $\delta_{sp}$  and one for  $\Delta p$ ), the most delicate is chosen as the applied control routine. This entails that the 'fine' routine is favoured over the other two, while the 'normal' routine is selected over the 'crude' routine.

Table 3.1.1 - control routines

	Unit	Crude	Normal	Fine
Relative delta set point	Nm <sup>3</sup> /h	$\delta_{sp} > 0,5$ of $\delta_{sp} < -0,5$	$0,25 < \delta_{sp} < 0,5$ of $-0,25 < \delta_{sp} < -0,5$	$0,1 < \delta_{sp} < 0,25$ of $-0,1 < \delta_{sp} < -0,25$
Pressure difference	Bar	0 - 1,0	1,0 - 2,0	$\Delta p > 2,0$

Then the position of the valve is taken into account. On the basis hereof and the selected control routine, the amount of increments that the position of the valve is changed with, is looked up in Table 3.1.2. An increment is one hundredth of one degree.

Table 3.1.2 - incremental adjustment

Position of the valve (incr.)	Factor	Crude (incr.)	Normal (incr.)	Fine (incr.)
1201-2000	Small (1x)	100	50	25
2001-4000	Average (2x)	200	100	50
4001-7800	Large (4x)	400	200	100

A dead valve stroke of 1200 increments is applied here, which also is in effect as free valve stroke above 7800 increments. When  $\delta_{sp}$  is positive, the valve position is increased with the amount of increments corresponding to the control routine and position of the valve. When  $\delta_{sp}$  is negative, the valve position is decreased.

For example: there is a  $Q_m$  of 1150 Nm<sup>3</sup>/h, at a  $Q_{sn}$  of 1000 Nm<sup>3</sup>/h,  $\Delta p$  of 1,8 bar and valve position of 30° (3000 increment).  $\delta_{sp}$  amounts -0,15. The  $\delta_{sp}$  suggested routine is 'fine' and the  $\Delta p$  suggested routine is 'normal'; the selected control routine is thus 'fine'. Table 3.1.2 gives an incremental

adjustment of 50 at routine 'fine' for this valve position. Since  $\delta_{s,p}$  is negative, the valve needs to close with an incremental adjustment of -50. The new valve position is 2950.

### 3.1.1 Parameter values

#### 3.1.1.1 Relative delta set point

Together with the stakeholders of the demonstration project it was determined that the flow through the valve should not deviate more than 10% from the set point. The least delicate control routine should only be used when there is a large deviation between flow through the valve and set point, of more than 50%. This is found to be the case when the set point is changed; the valve should be able to quickly open or close in that case to reach the new set point. The other two settings should be used when the set point just deviates more than the tolerated amount from the set point and when the pressure difference across the valve rapidly decreases due to the morning consumption peak. These segments are separated at a deviation of 25%.

#### 3.1.1.2 Pressure difference

Regarding pressure difference, the valve should be able to respond quickly when there is a peak in consumption, at which moment the pressure difference across the valve is minimal. The value chosen for this boundary is 1 bar, since no series with constant pressure differences below 1 bar have been found in the data from the 2013 demonstration project (except for pressure differences of less than 0,1 bar, at which moment flow through the valve stagnates); the first time series of at least half an hour of constant pressure difference was found at 1 bar. The other boundary is chosen at 2 bar, since the gas receiving stations are more likely to supply gas when the pressure difference exceeds 2 bar, while they seldom supply gas to the grid when the pressure difference is below 2 bar.

#### 3.1.1.3 Position of the valve

The valve position factor values are separated at 2000 increments, since up to that point in the valve characteristic shown in Figure 4.2.1 behaves in a non-linear trend, while from 2000 increments on, it does show a linear trend. Valve positions of less than 2000 increments, which is the lower 12% of the operational range of the valve, are only common at low set points (lower than 500 Nm<sup>3</sup>/h). Higher set points correspond with valve positions up to 4000 increments. The valve usually only exceeds a position of 4000 increments when the pressure difference across the valve is small. The valve should then be able to respond rapidly because a sudden increase in pressure difference can occur as a result of a peak in consumption.

#### 3.1.1.4 Incremental change


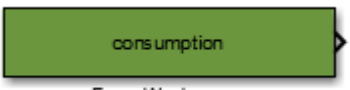




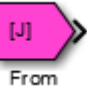



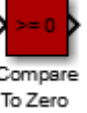
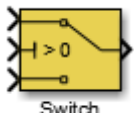
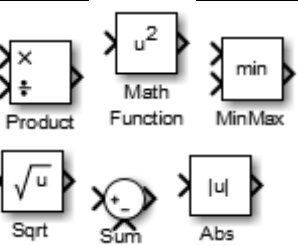
The incremental changes of 100, 50 and 25 have been chosen in such a way that the flow through the valve doesn't skip a control action (go from 'crude' at  $t_{n-1}$  to 'fine' at  $t_n$ ). It should always pass from control action 'crude' through 'normal and thereafter by 'fine' to the point where no further action is needed. It does not have to start with applying a 'crude' setting though.

## 3.2 Simulation of the control concept

In order to test the functioning of the constant flow control, the entire system in which it will operate has been modelled. This model is split up in three sections: the gas grid, the control concept and the valve flow.

The model is built using the Simulink environment in MATLAB software. Table 3.2.1 shows a legend of the blocks and colours in the model. The three sections of the model (gas grid, control concept and valve flow) are first shown in their entirety, after which they are broken down into segments in order to explain the functioning of the model in a more clear manner.

Table 3.2.1 - Legend of model blocks

Simulink blocks	Explanation block	Explanation colour
 Scope	'Scope' blocks display time domain signals	All orange blocks are scopes containing data of input signals
 From Workspace	'From Workspace' blocks read data values specified in time series	All dark green blocks are constants and variables that are not influenced by the flow through the valve
 Saturation	'Saturation' blocks limit the input to the upper and lower saturation values	All red blocks are parts of the gas receiving station
 Constant	'Constant' blocks contain a specified constant value	All black blocks are unchangeable mathematical constants necessary for the functioning of the model
 Fcn	'Fcn' blocks contain defined mathematical functions	All green blocks are part of the Green Gas feed-in
 Goto	'Goto' blocks send signals to 'From' blocks with the same tag	All cyan blocks are concerned with the relative delta set point
 From	'From' blocks receive signals from the 'Goto' block with the specified tag	All magenta blocks are concerned with the flow through the SG3 system
 Data Store Write	'Data Store Write' blocks write values to the specified data store	All light blue blocks are concerned with the position of the valve
 Data Store Read	'Data Store Read' blocks read values from the specified data store	All blue blocks are concerned with the pressure in the gas grid
 Data Store Memory	'Data Store Memory' blocks define a memory for the specified data store	All grey blocks are concerned with the constant flow control
 Compare To Zero	'Compare To Zero' blocks determine how a signal compares to zero	All maroon blocks are concerned with the pressure difference across the valve
 Switch	'Switch' blocks pass through input 1 when input 2 satisfies the selected criterion; otherwise, it passes through input 3	All yellow blocks contain changeable parameter values
	These mathematical operation blocks are also used throughout the model	All white blocks are mathematical operators



### 3.2.1 Gas grid

The gas grid model section depicted in Figure 3.2.1 is split up in five segments: gas receiving station delivery, Green Gas feed-in, gas consumption, buffer and pressure.

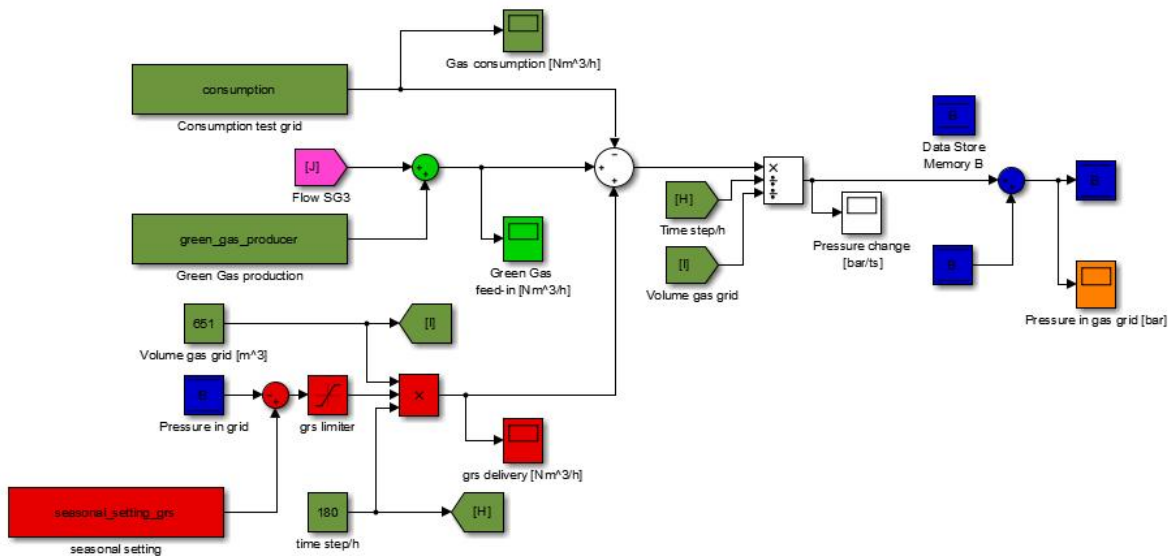


Figure 3.2.1 - model of gas grid

#### 3.2.1.1 Gas receiving station delivery

The gas receiving station is responsible for keeping the pressure in the gas grid at a minimum pressure. It is displayed in Figure 3.2.2.

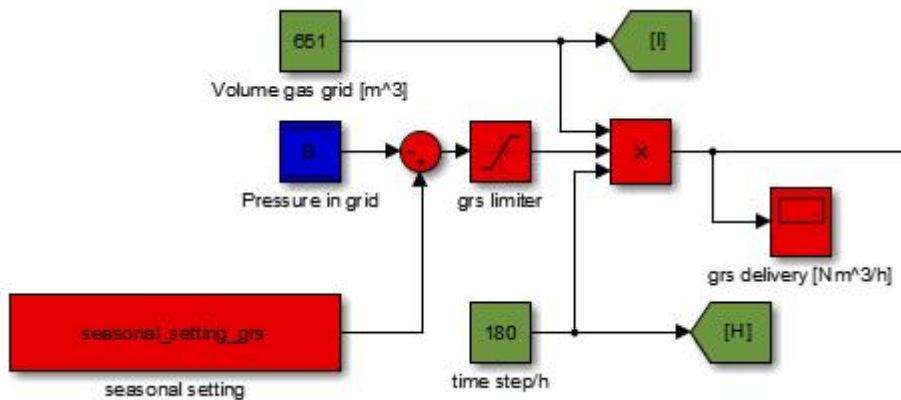


Figure 3.2.2 - model of gas receiving station delivery

The 'seasonal setting' block contains data on the minimum pressure in the gas grid, which in 2013 was 4,5 bar relative pressure and in 2016 will be 5 bar; this is the pressure in the grid with respect to the normal pressure. The actual relative pressure in the gas grid is subtracted from the seasonal setting. When this outcome is negative, which is the case when the pressure in the grid is higher than the seasonal setting, it is saturated to zero by the 'grs limiter'. The outcome is multiplied with the volume of the gas grid and the amount of time steps in an hour, which results in the gas delivery by the gas receiving station in normal cubic meters per hour. The system determines a new control action every 20 seconds, so the amount of steps in an hour is 180.

The volume of a gas grid is obtained by filling the grid with water, which is an incompressible fluid. The size of the buffer in cubic meters is thus calculated using the water volume in  $m^3$  of the Bunschoten-Eemnes gas grid. The water content of the Bunschoten-Eemnes gas grid was found to be  $651 m^3$ .<sup>2</sup>

3.2.1.2 Green Gas feed-in

The Green Gas feed-in is determined by taking the sum of the input of the Green Gas feeders in the grid, as shown in Figure 3.2.3. The feed-in of the Green Gas producer is measured in  $Nm^3/h$  every time step, while the feed-in of Green Gas by the SG3 system is obtained from the valve flow section of the model in paragraph 3.2.3.

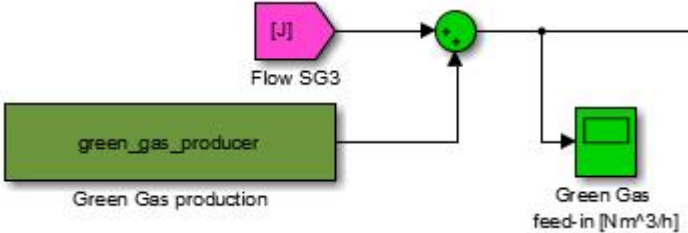


Figure 3.2.3 - model of Green Gas feed-in

3.2.1.3 Gas consumption

The gas consumption in the grid shown in Figure 3.2.4 is not measured, but is estimated on historical data by adding up the gas delivery by the gas receiving station and the Green Gas feed-in, while subtracting the amount of buffered gas. The amount of buffered gas is determined by multiplying the change in pressure in the grid with the volume of the grid.

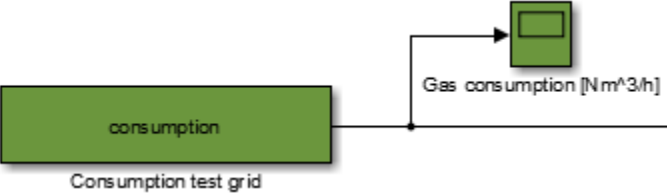


Figure 3.2.4 - model of gas consumption

3.2.1.4 Pressure change

The gas consumption is subtracted from the Green Gas feed-in and gas delivery by the gas receiving station. This gives the flow of gas entering or exiting the grid in normal cubic meters per hour. This flow is divided by the amount of time steps in an hour to acquire the flow of gas per time step, which is divided by the volume of the gas grid to acquire the change in pressure resulting from the gas flow. This is illustrated in Figure 3.2.5.

<sup>2</sup> Verified by Stedin

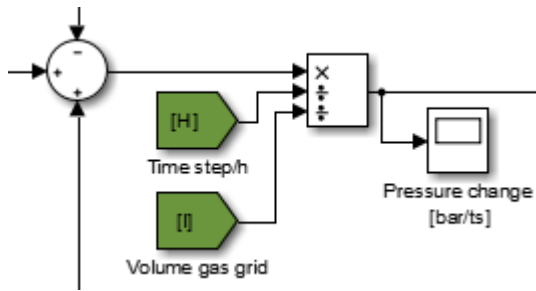


Figure 3.2.5 - model of pressure change

### 3.2.1.5 Pressure in gas grid

The change in pressure obtained from 3.2.1.4 is added to the grid pressure of the former time step to acquire the new grid pressure shown in Figure 3.2.6.

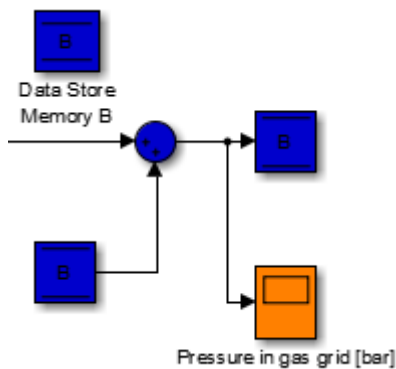


Figure 3.2.6 - model of pressure in gas grid

## 3.2.2 Control concept

The control concept model section in Figure 3.2.7 is split into nine segments: relative delta set point, delta set point setting, pressure difference, pressure difference setting, control setting, valve position setting, sign delta set point, valve position change and valve position.

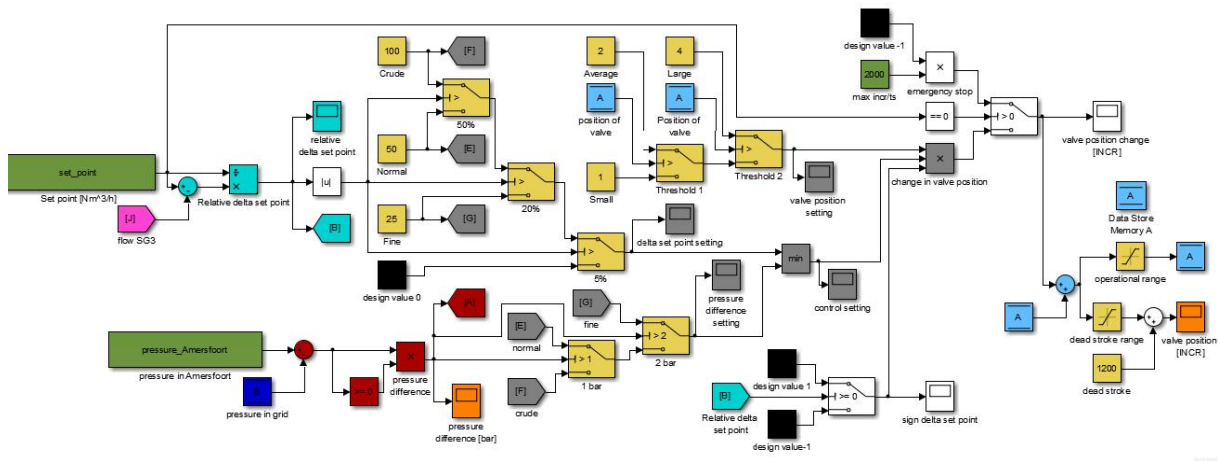


Figure 3.2.7 - model of control concept

### 3.2.2.1 Relative delta set point

The absolute difference between the set point and the measured flow is divided by the set point through equation ( 32 ) in order to obtain the relative delta set point in Figure 3.2.8.

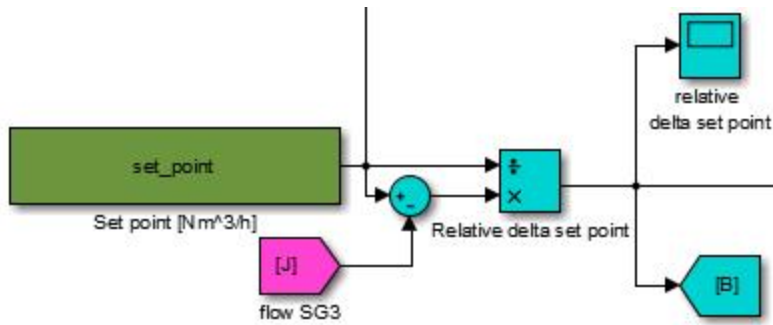


Figure 3.2.8 - model of relative delta set point

### 3.2.2.2 Delta set point setting

The absolute value of the relative delta set point is taken to determine the setting of the control for the relative delta set point by use of Table 3.1.1 in paragraph 3.1. If the relative delta set point deviates more than 50% of the set point, the setting will be 'crude'. When it differs in between 20% and 50% of the set point the valve response is 'normal' and when it varies between 10% and 20% of the set point the control action is 'fine'. When the relative delta set point differs less than 10% of the set point, there will be no action from the valve. The corresponding values for the change in increments obtained from Table 3.1.2 are also shown in Figure 3.2.9.

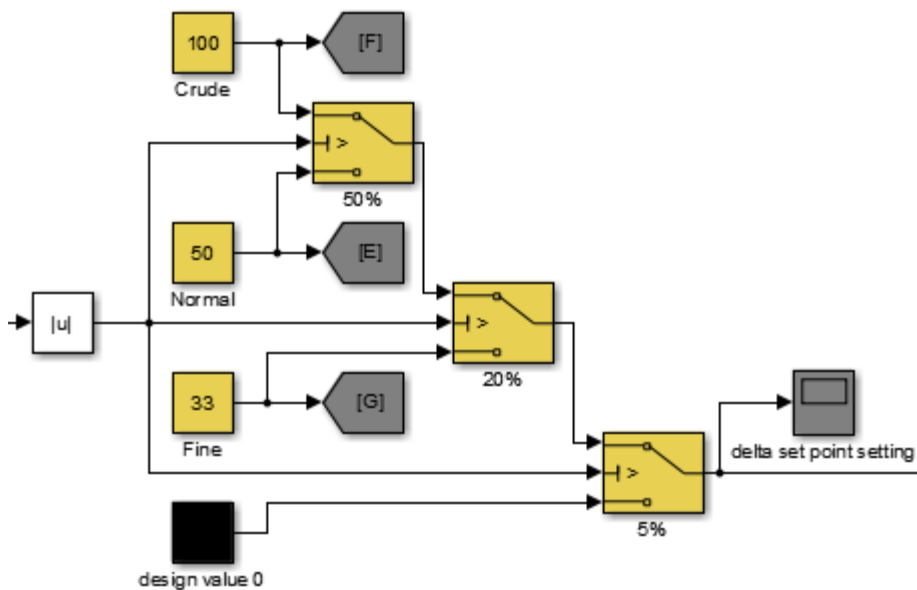


Figure 3.2.9 - model of delta set point setting

### 3.2.2.3 Pressure difference

The pressure difference across the valve is obtained by subtracting the pressure in the grid from the pressure in the grid of Amersfoort through equation ( 17 ). In the model segment illustrated in Figure 3.2.10 is checked whether the pressure difference is negative, which would mean that the pressure of the grid in Amersfoort would be lower than that of the test grid. In this case a return flow would occur through the non-return valve as described in chapter 2.3. The effective pressure difference over the control valve is then zero.

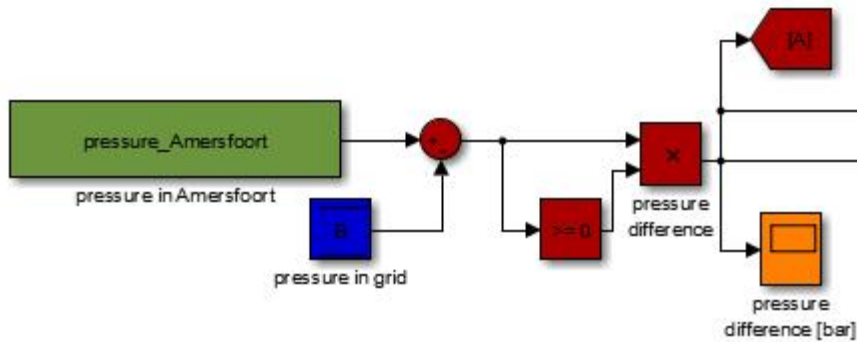


Figure 3.2.10 - model of pressure difference

### 3.2.2.4 Pressure difference setting

The pressure difference across the valve is used to obtain the setting of the control for the pressure difference using Table 3.1.1. This is displayed in Figure 3.2.11. If the pressure difference is smaller than 1 bar, the setting will be 'crude'. When it lays in between 1 and 2 bar, the valve response is 'normal' and when the pressure difference is larger than 2 bar, the control action is 'fine'.

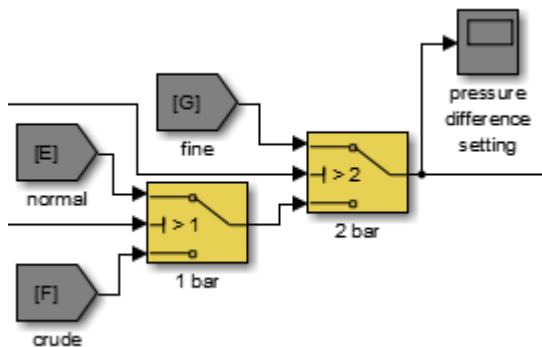


Figure 3.2.11 - model of pressure difference setting

### 3.2.2.5 Control setting

The control actions from the relative delta set point and pressure difference obtained from paragraphs 3.2.2.2 and 3.2.2.4 are compared and the most delicate control action is chosen, as is described in paragraph 3.1. This segment of the model is represented in Figure 3.2.12.

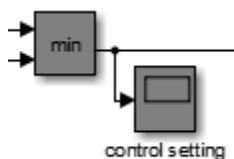


Figure 3.2.12 - model of control setting

### 3.2.2.6 Valve position factor

The valve position factor is obtained from the position of the valve in the operational range of the valve, as shown in Figure 3.2.13. When the valve position is smaller than 2000 increments, the factor is 'small'. When it lays in between 2000 and 4000 increments, the valve position factor is 'average' and when the valve position is larger than 4000 increments, the factor is 'large'.

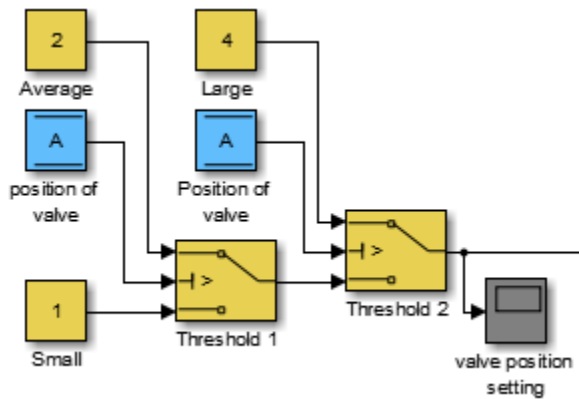


Figure 3.2.13 - model of valve position factor

### 3.2.2.7 Sign delta set point

In order to determine whether the valve needs to be opened or closed, it is checked whether the relative delta set point is larger than (or equal to) zero, in which case it will return a value of 1. When it is smaller than zero, it will return a value of -1. This part of the model is shown in Figure 3.2.14.

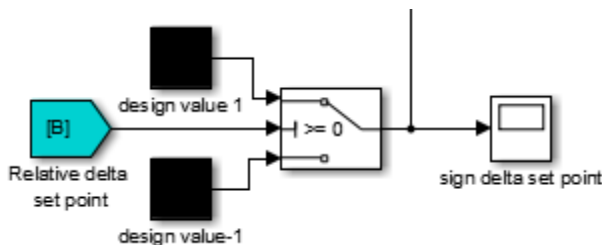


Figure 3.2.14 - model of sign delta set point

### 3.2.2.8 Valve position change

The control setting obtained from paragraph 3.2.2.5, the valve position factor from paragraph 3.2.2.6 and the value for the direction of the operation from paragraph 3.2.2.7 are multiplied to obtain the change in valve position in increments (one degree equals 100 increments). This is explained in paragraph 3.1 and illustrated in Figure 3.2.15.

This position change can be overruled by an emergency stop, which is activated when the set point is equal to zero. When this emergency stop is activated, the valve will close as fast as possible. The fastest valve operation speed is one degree per second, which equals 2000 increments per time step.

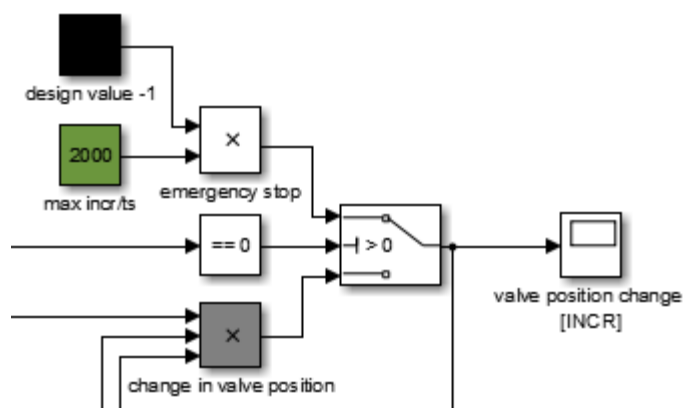


Figure 3.2.15 - model of valve position change

### 3.2.2.9 Valve position

The change in valve position obtained from 3.2.2.8 is added to the valve position of the former time step to acquire the new valve position. In Figure 3.2.16 is shown that the valve position is saturated in the 'operational range' block, so it cannot exceed the maximal operational range. This is the value used in other parts of the model when the position of the valve is mentioned. The dead valve stroke is added in another branch to show the absolute valve position.

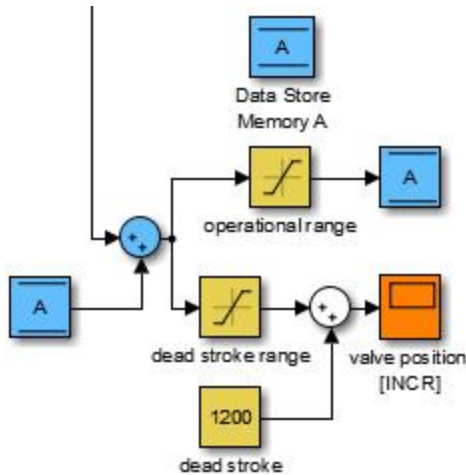


Figure 3.2.16 - model of valve position

### 3.2.3 Valve flow

The valve flow model section depicted in Figure 3.2.17 is split into two sections: calculated flow and measured flow.

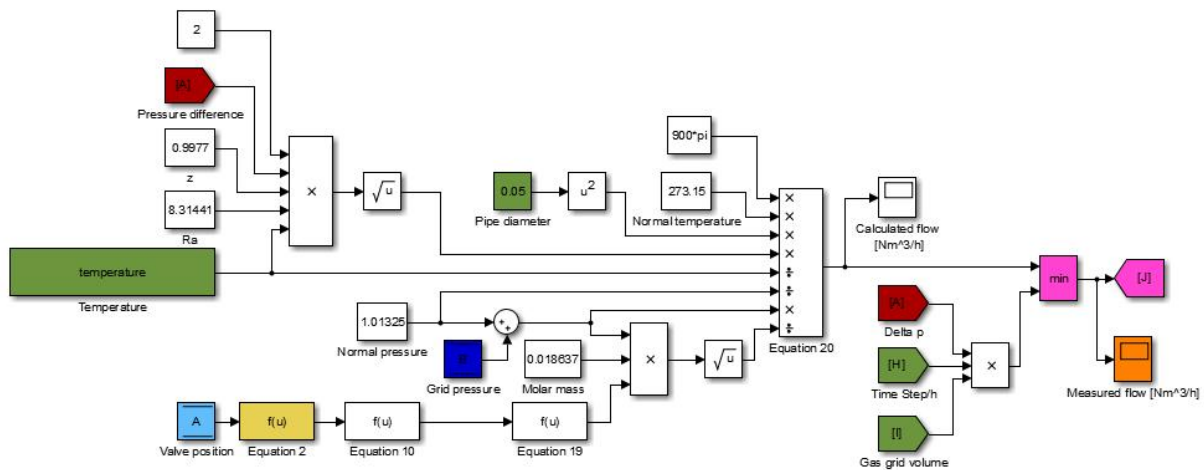


Figure 3.2.17 - model of valve flow

#### 3.2.3.1 Calculated flow

In order to calculate the flow through the valve, the theory from sections 2.1 and 2.2 is implemented into the model through equations ( 2 ), ( 10 ) and ( 19 ) in the 'Fcn' blocks in Figure 3.2.18. The gas flow through the valve is determined from the temperature of the gas in the grid, the pressure in the grid, the pressure difference across the valve and the position of the valve according to equation ( 20 ).

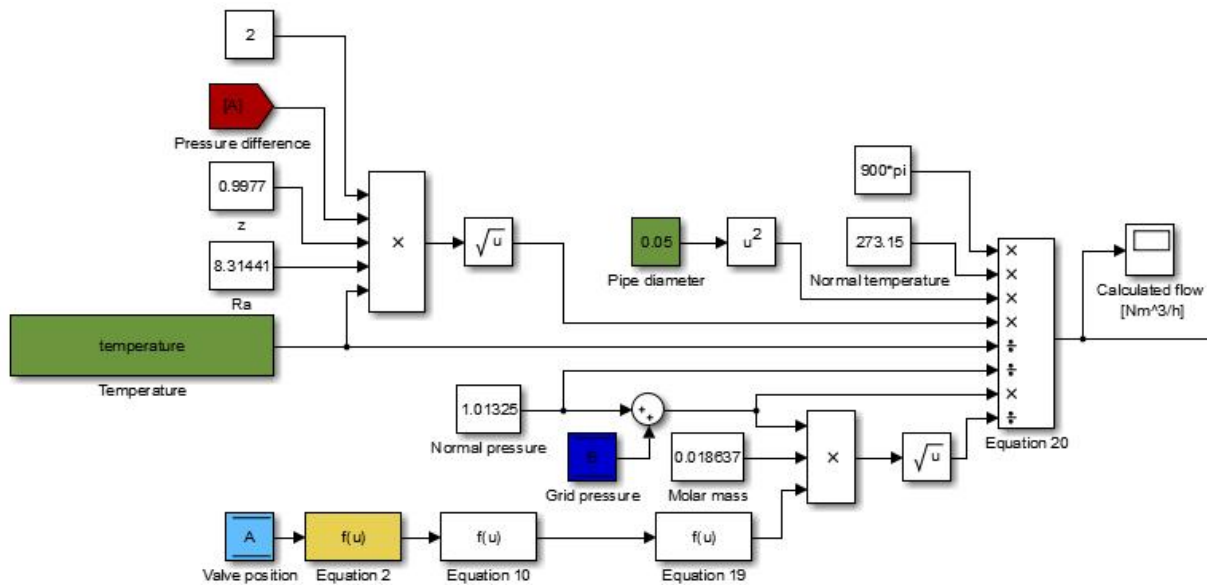


Figure 3.2.18 - model of calculated flow

### 3.2.3.2 Measured flow

Since there is a delay in the input signals 'position of the valve' and 'pressure in grid' of respectively one and two time steps, it is possible that the calculated flow is larger than the actual buffer size at that moment. The flow limitation calculation is added to this model segment, shown in Figure 3.2.19, which calculates the flow that would fill the entire available buffer in one time step. The system always favours the smallest flow, so if the buffer flow is smaller than the calculated flow, the buffer flow will be the measured flow.

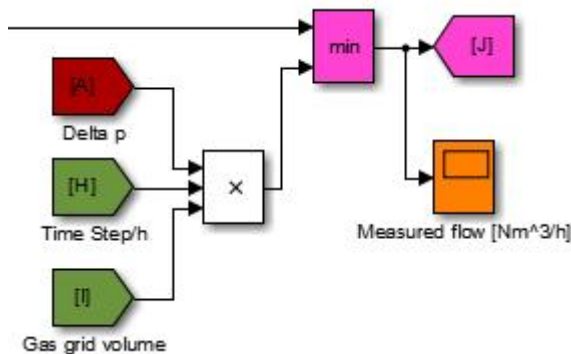


Figure 3.2.19 - model of measured flow

## 3.3 Field test

In order to create a controlled test environment, the gas grid of Bunschoten-Eemnes is isolated from the gas grid of Amersfoort. The SG3 grid (Bunschoten-Eemnes) is fed by two gas receiving stations, a Green Gas producer in Spakenburg and the SG3 station connected to the grid of Amersfoort, which will be used to simulate a second Green Gas producer. The SG3 station is remotely operated by Stedin.

The field test has taken place in week 25 in June 2016. The pressure in the gas grid has for the first time been lowered to 5 bar relative pressure by Gasunie. During the initial field tests a problem with feed-in of Green Gas was experienced due to the lower pressure in the gas grid. As a result, the minimal relative pressure reached during this demonstration will be 5 bar instead of the 4,5 bar that has been realised in the 2013 field tests.



## 4 Results

### 4.1 Dead valve stroke

In order to determine the dead valve stroke, data from the 2013 demonstration project is used. This dataset contains measurements for every two minutes from 2-8-2013 8:26 to 15-9-2013 23:58. The variables that are included are the position of the valve, the pressure in the test grid, the pressure difference across the valve and the gas flow through the valve. The entire set consists of 31770 data points, of which 30058 are relevant. Data points have been filtered out because they are either incomplete or because the valve was malfunctioning.

The first sensible data points are located at  $\pm 12^\circ$ . For all angles smaller than  $12^\circ$  no gas flow is measured, while for all angles greater than  $12^\circ$  there is a measured gas flow through the valve. This also applies to the fully open angle of the valve, which is thus  $78^\circ$ . For all angles greater than  $78^\circ$  no more additional gas flows through the valve in comparison to angle  $78^\circ$ . This leaves an operational range of the valve of 66 degrees.

### 4.2 Characteristic of the valve

The characteristic for the ball valve has been determined by applying the theory described in chapter 2.1.2 for multiple relative angles  $h$ . The result is shown in Figure 4.2.1 and is in line with ball valve characteristics found in literature, such as Chern et al. (2007).

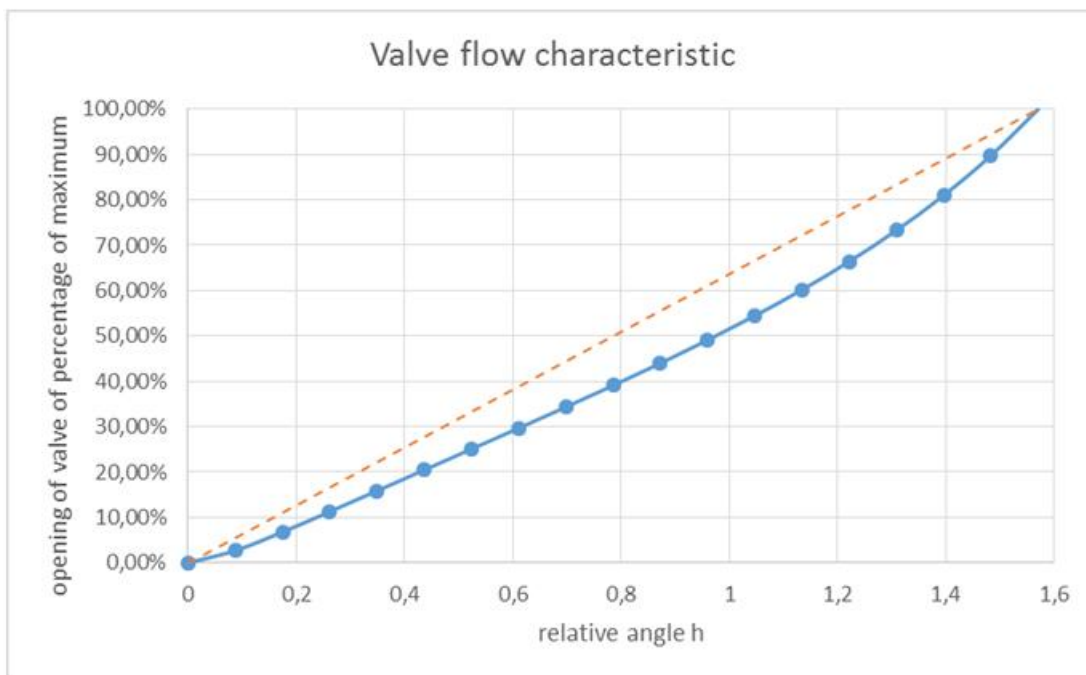


Figure 4.2.1 - ball valve flow characteristic

### 4.3 Sensitivity of control concept

A sensitivity analysis has been conducted on the impact of the input signals defined in Table 2.2.1 on the projected flow through the valve. The sensitivity of the input signals is tested to flow through the valve  $Q_m$ . The sensitivity of these input signals is shown in Figure 4.3.1.

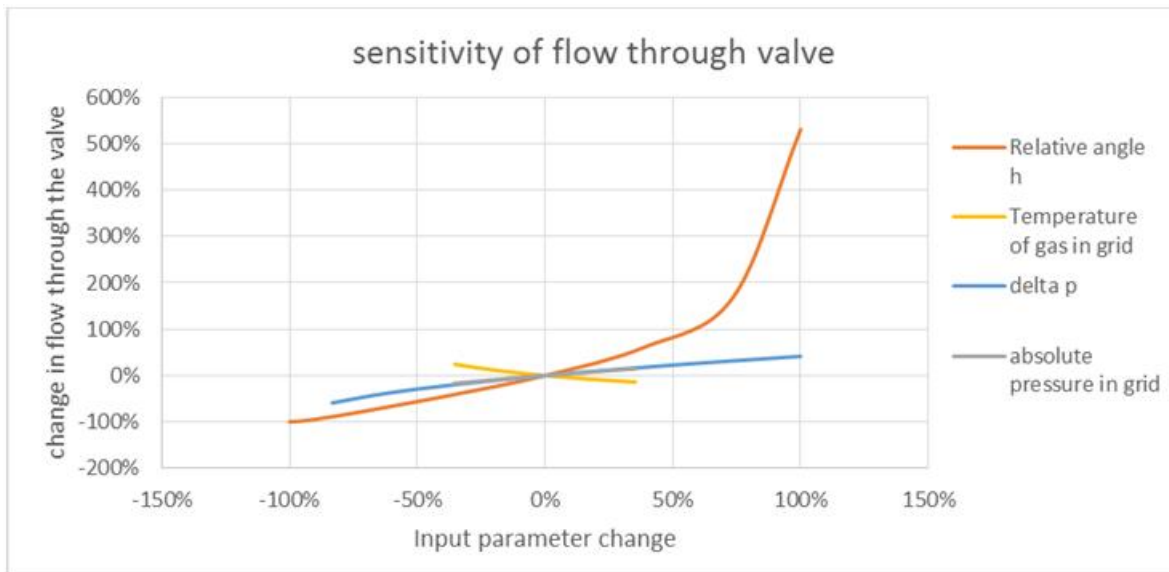


Figure 4.3.1 - sensitivity analysis of input signals on the flow through the valve

As can be seen in Figure 4.3.1, is that the flow through the valve is most sensitive to changes in the relative angle  $h$ . However, the flow through the valve is very sensitive when the valve is almost fully open, what makes operation of the valve in this range complicated. Next to this, the flow through the valve is somewhat sensitive to changes in temperature, changes in the pressure in the grid and pressure difference across the valve.

#### 4.4 Operation of the valve

The model developed in paragraph 3.2 has been run on a set of input signals from the 2013 field test. These input signals are the gas consumption, seasonal setting of the gas receiving station, green gas production, the set point, the pressure of the grid in Amersfoort and the temperature of the gas.

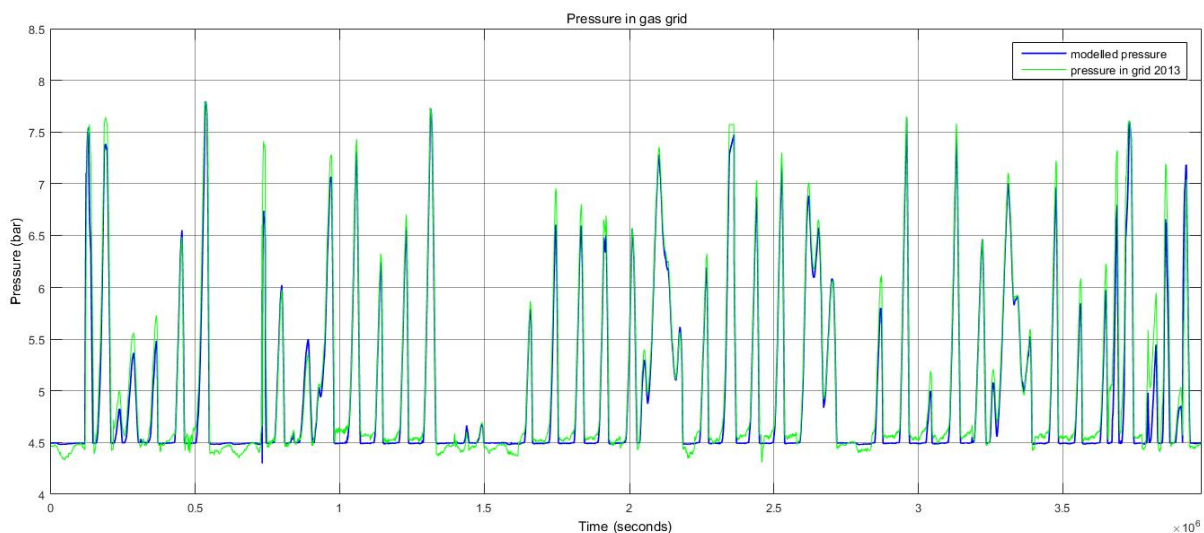


Figure 4.4.1 - pressure in the test grid

The development of the pressure in the grid can be seen in Figure 4.4.1. What can be seen is that the modelled pressure follows the historical pressure quite well. It never exceeds the 8 bar limit in the gas grid and only once falls significantly below 4,5 bar. Overall, the new control concept seems better able to keep the pressure in the grid from falling below 4,5 bar. The model overall fits very well with the

trend shown in the historical data, although the peak pressures are higher in the historical dataset. Next to this, the first week shows a much higher modelled pressure than measured pressure.

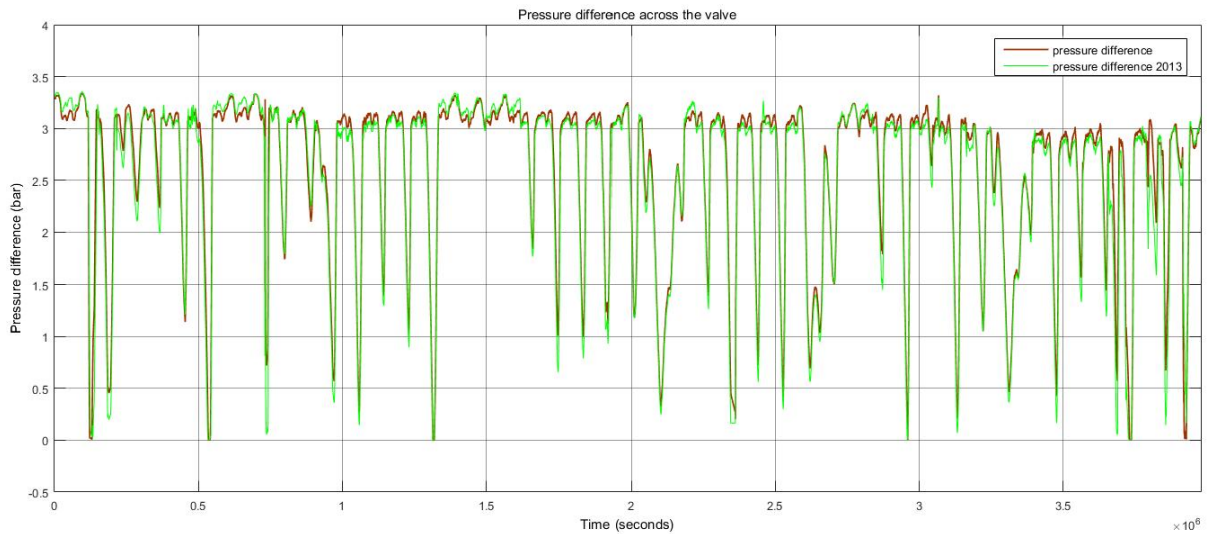


Figure 4.4.2 - pressure difference across the valve

The pressure difference in Figure 4.4.2 follows the same trend as the pressure of the grid in Figure 4.4.1. What can be seen is that the modelled pressure difference follows the historical pressure trend and it never falls below 0 bar. As is the case for the pressure in the grid, the model overall fits very well with the trend shown in the historical data, except for the peak pressure differences, which are higher in the historical dataset, and the first week, which shows a much higher modelled pressure difference.

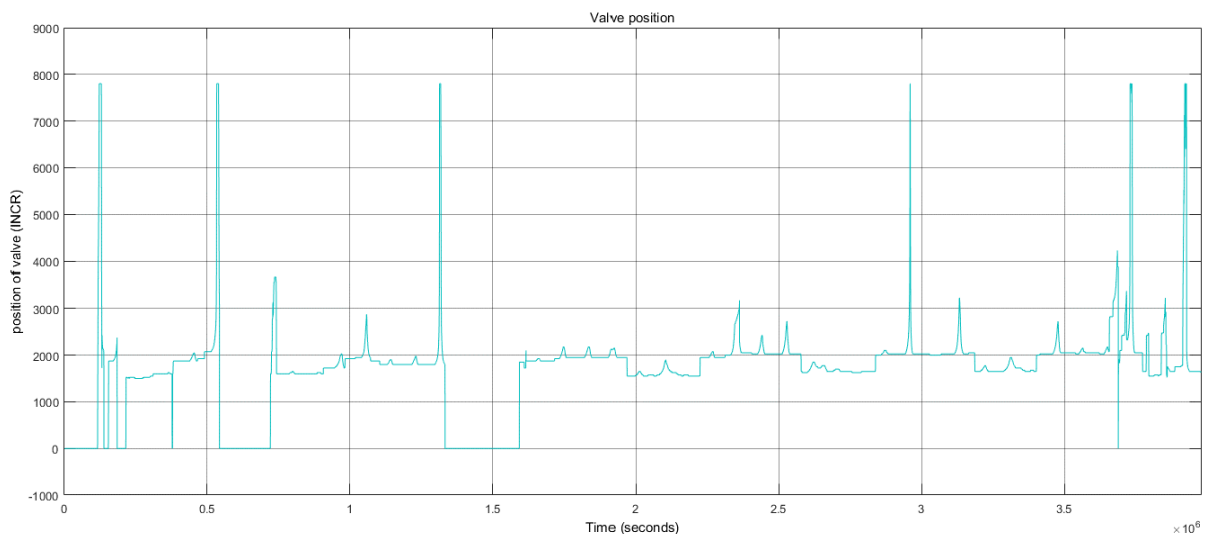


Figure 4.4.3 - position of the valve

Figure 4.4.3 shows the progress of the simulated valve position over the 1,5 month test period. As was to be expected, the valve position never exceeds its maximal operational position at 7800 increments. Furthermore, the overall trend shows that the valve position trends to a peak every day. This is because of a matching decline in pressure difference across the valve, which means that less gas flows through the valve at that position, so the valve needs to open more. When more gas is consumed in the grid, the pressure difference increases, meaning more gas flows through the valve, so the valve needs to close.

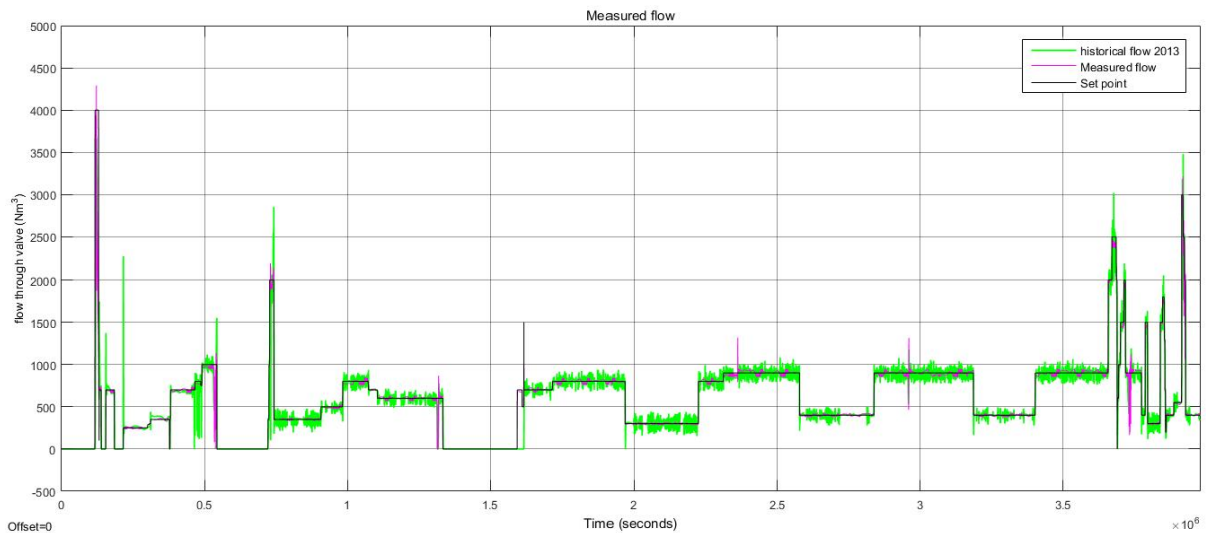


Figure 4.4.4 - measured flow through the valve

Figure 4.4.4 shows the measured flow of gas through the valve as well as the set point at that time. What can be seen is that the measured flow of the model and the historical flow are both equally able to keep up with the set point. However, the modelled flow shows a much more constant trend and lies much more close to the set point than the historical flow. This means that the new control algorithm is able to follow the set point better than the old algorithm.

#### 4.5 Valve behaviour in critical situations

Over the course of a day, there are two peaks in gas consumption: a large peak in the morning and a small peak in the evening. The large peak in the morning is seen as the most critical factor in assessing valve behaviour, since the pressure difference across the valve will suddenly go from (almost) zero to maximum in a short time period. The most steep increase in pressure difference during the 2013 test was found on 4-9-2013. The graphs show the trend in the gas grid from 3-9-2013 12:00 until 4-9-2013 12:00.

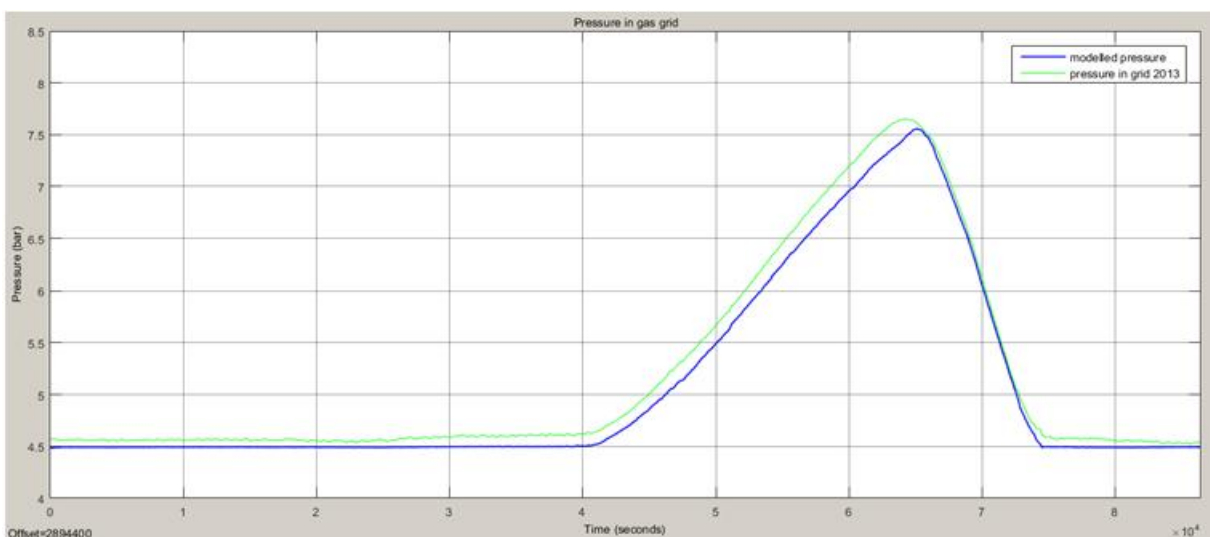


Figure 4.5.1 - pressure in the gas grid on 3-9-2013/4-9-2013

As can be seen in Figure 4.5.1, the pressure in the gas grid slowly starts building up from 23:30 on 3-9-2013. At around 6:00 on 4-9-2013 the pressure in the gas grid reaches its maximum value of 7,65 bar,

while the modelled pressure has a slightly lower maximal pressure. Two and a half hours later, at 8:30, the pressure in the gas grid has fallen back to 4,5 bar again.

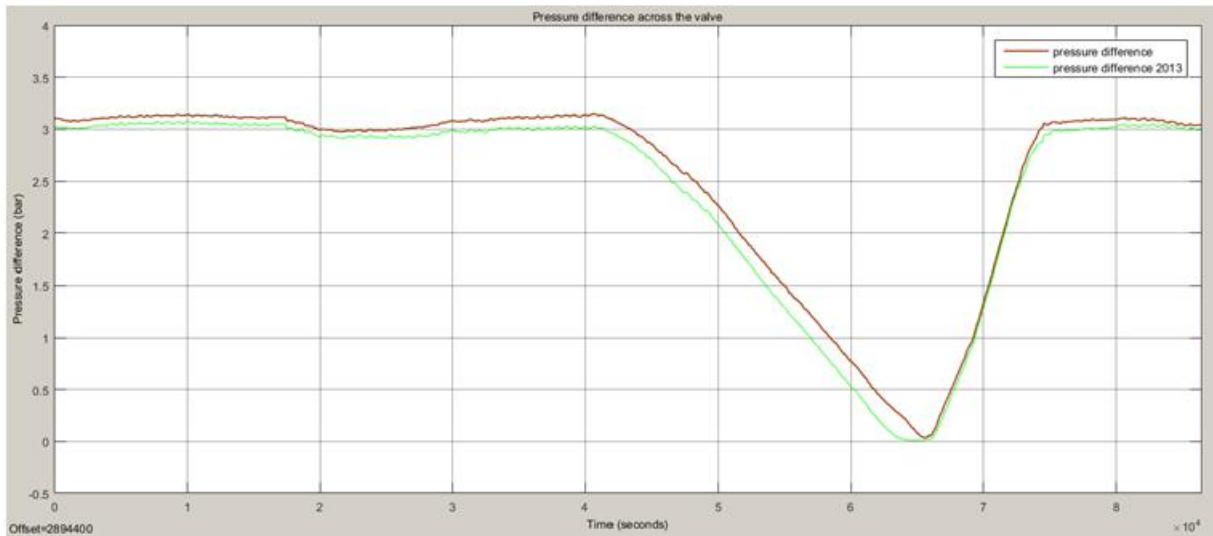


Figure 4.5.2 - pressure difference across the valve on 3-9-2013/4-9-2013

Following up on the trend of the pressure in the gas grid, the pressure difference shows a corresponding trend, as seen in Figure 4.5.2. The pressure difference is zero for about 20 minutes, while the modelled pressure difference does not reach a pressure difference of zero. Eventually, the pressure difference starts to increase rapidly and in two and a half hours, it has increased to 3 bar. The small evening peak on 3-9-2013 can also be seen in the graph.

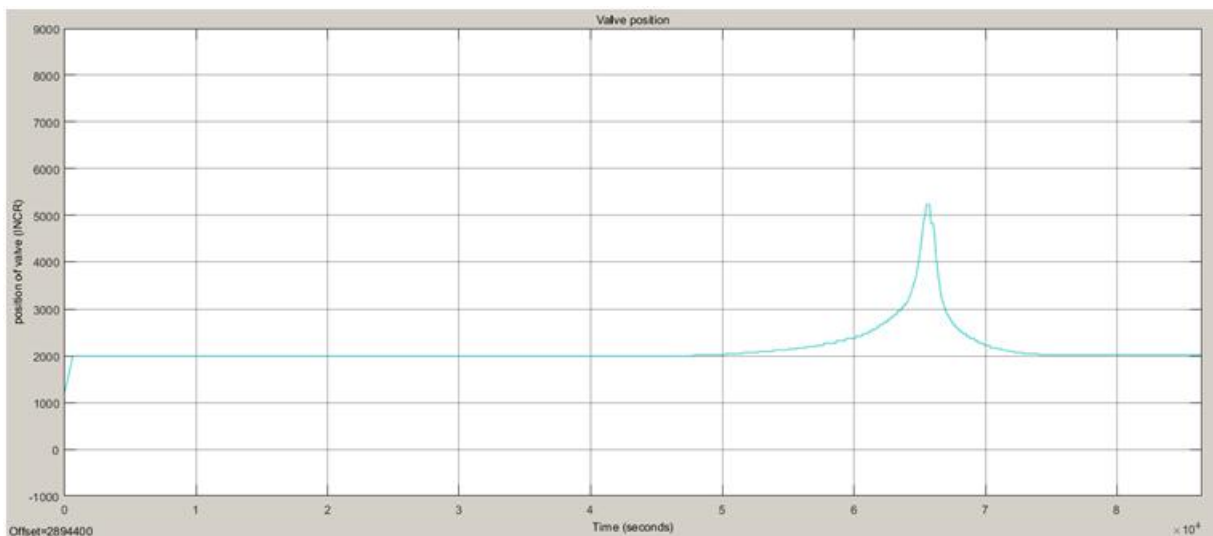


Figure 4.5.3 - position of the valve on 3-9-2013/4-9-2013

Because of the decrease in pressure difference, the valve starts to open up at an increasing trend from 4-9-2013 1:00. It reaches its peak at around 6:00, at which moment the pressure difference is close to zero. It starts to close rapidly from 6:20 on and reaches a stable valve position at 8:30, at which moment the pressure in the grid is stable.

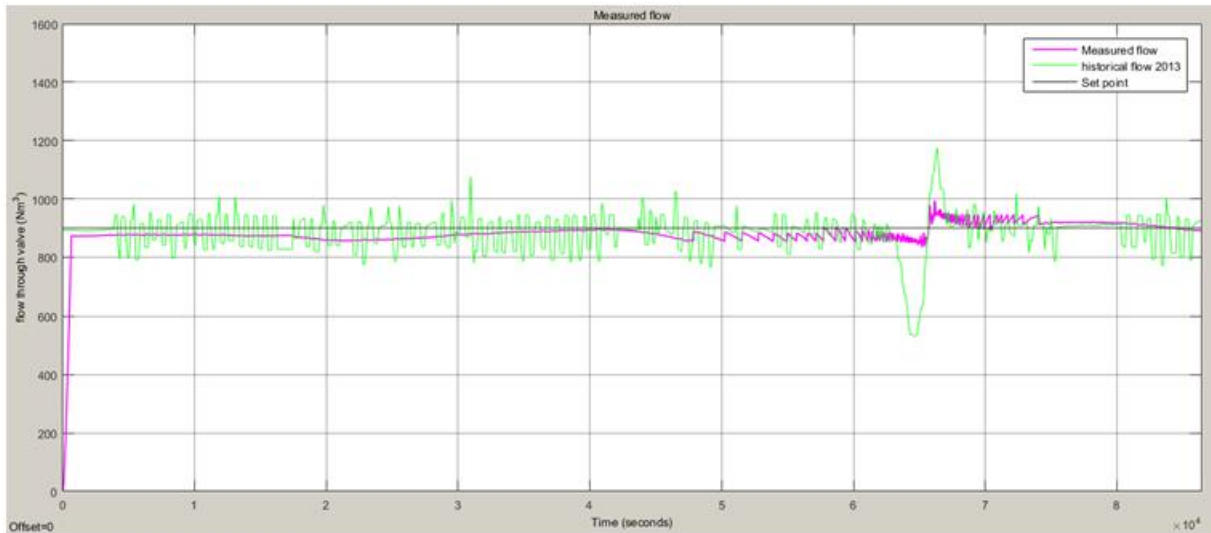


Figure 4.5.4 - Measured flow through the valve on 3-9-2013/4-9-2013

The flow through the valve, shown in Figure 4.5.4, reveals the difference in performance between the old control used in 2013 and the new control. The first observation is that the modelled measured flow is much more constant than the historical flow on 3-9-2013. When the pressure difference starts to decline, the response of the valve is able to keep the flow close to the set point, up to the point where the pressure difference is nearly zero at 6:00. After 20 minutes, the pressure difference starts to rapidly increase, at which moment the valve starts to close. The new control responds more quickly than the old control algorithm, without skipping over the set point.

#### 4.6 Field test

The results of the field test are shown in Figure 4.6.1. What can be seen is that the flow through the valve shows signs of its old habit between 20-6 16:00 and 21-6 16:00, while it is able to follow the set point constantly between 21-6 16:00 and 22-6 16:00. This is because between 20-6 16:00 and 21-6 16:00, the tolerated deviation from the delta set point was set to 5%, as this appeared to be reachable from the model results. Since the valve behaved undesirably with this parameter, the parameter was changed to 10%, which results in the desired behaviour of the valve.

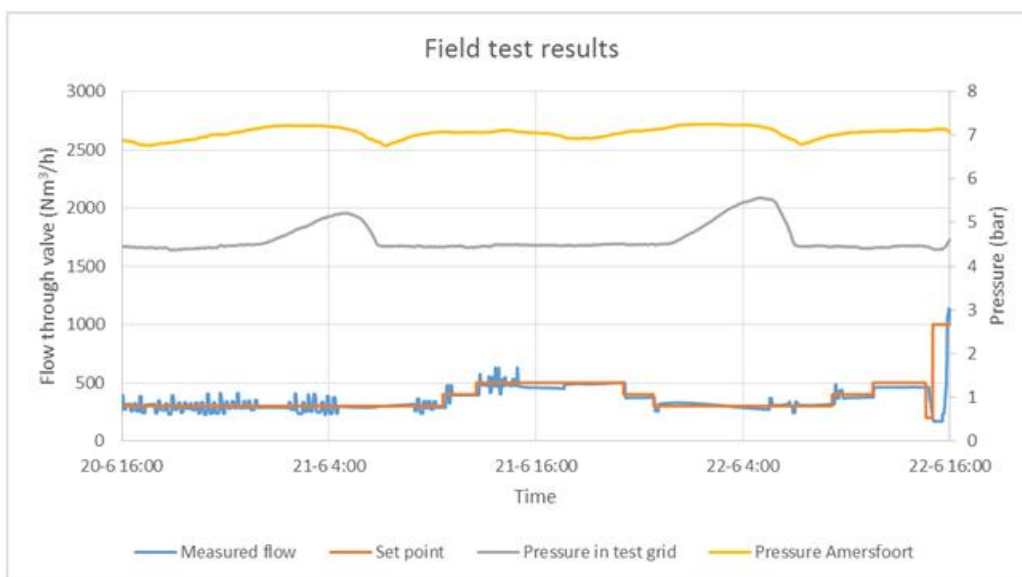


Figure 4.6.1 - results of field test

## 5 Discussion

### 5.1 Methodology

The initial goal of this research was to calculate the flow of gas through the valve using the theory described in chapter 2. However, when comparing it to the data from the field test in 2013, it showed that there was a large unexpected discrepancy between the calculated flow by the model and the measured flow through the valve.

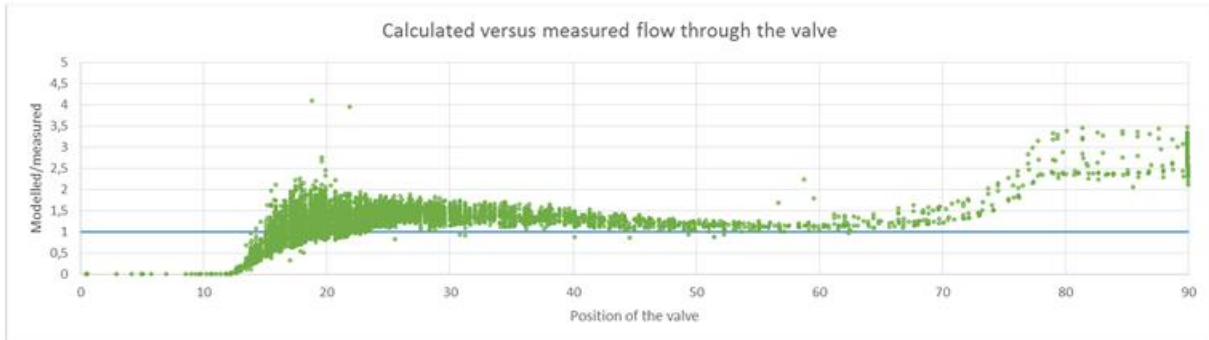


Figure 5.1.1 - calculated flow versus the measured flow through the valve for the 2013 field test

The offset between the calculated flow and the measured flow for the field test in 2013 is shown in Figure 5.1.1. It can be seen that there is a clear offset between the modelled flow and the measured flow. What makes it more complex, is that there are several trends active in this figure. The most striking, however, is the 'cloud' of data points around the position of the valve at around 20 degrees. In order to get a better picture of what causes these data points to be located in a cloud rather than a line, the input signal expected to cause this behaviour, pressure difference over the valve, is isolated in Figure 5.1.2.

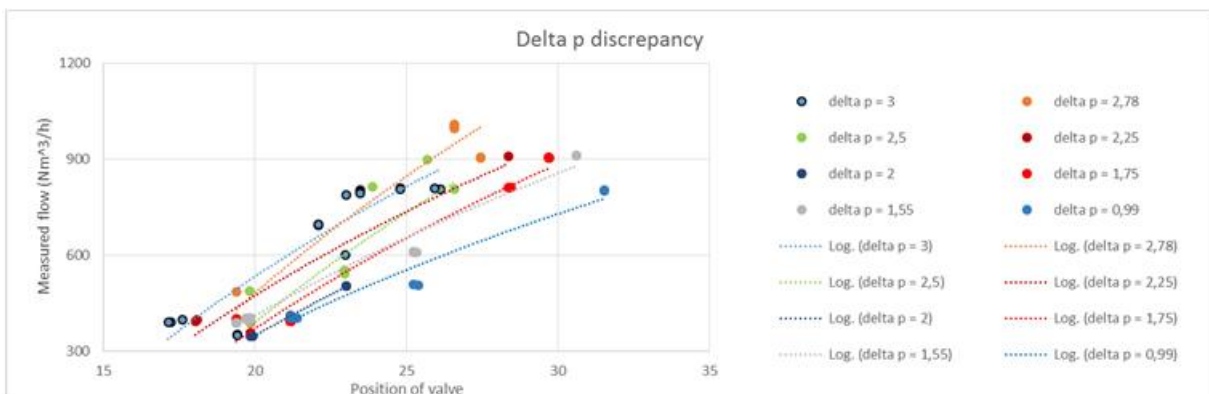


Figure 5.1.2 - data points grouped on pressure difference

Figure 5.1.2 shows the measured flow at certain positions of the valve for eight sets of pressure difference across the valve ( $\Delta p$ ). Within these eight sets, it was expected that the measured flow at a set position of the valve would always be higher for a larger pressure difference. As can be seen in Figure 5.1.2, this is not the case. This means that the basis of the entire method of having a calculated flow through the valve that is representable of the actual flow, is implausible. That is why in the end the solution of developing a new constant flow control was chosen.

### 5.2 General simplifications

The dead valve stroke is obtained through analysis of data of the 2013 demonstration project. The set-up of the SG3 system does not allow for direct measurement of the dead valve stroke. It is only

operated by giving in a set point for the SG3 system to provide a flow for. The system itself does not register flows of less than 100 Nm<sup>3</sup>/h.

The initial value for the 'fine' incremental change setting was 33 increments, but this proved to be too large to keep the flow constant during the modelled test. Therefore, this setting was scaled down to 25 increments.

After testing the new control algorithm in the model, it appeared to be possible to keep the flow through the valve within 5% of the set point. However, during the field test it was discovered that the flow meter cannot measure the flow through the valve quickly enough, since it provides a signal every time one m<sup>3</sup> of gas passes through it. This corresponds with about 500 Nm<sup>3</sup>/h, for which it can send a signal each minute. Since the control will provide an action for the valve regardless of whether the measured flow is an old signal, the lower boundary was kept at 10%.

## 5.3 Modelled environment

### 5.3.1 Model simplifications

Two gas receiving stations exist in the grid, while only one has been modelled. However, one of these gas receiving stations didn't deliver any gas during the 2013 field test, so implementing just one gas receiving station into the model should be sufficient. Despite this simplification, the model seems to be able to better maintain grid pressure than the SG3 system did according to the 2013 data. As can be seen in Figure F.1 in Appendix F, the modelled gas receiving station shows a similar trend in gas delivery as the historical delivery by the gas receiving stations, but a larger variation on this trend. Therefore, it might be that the response of the gas receiving station in the model is modelled too optimistic.

For the input signals pressure in the grid and position of the valve, the values at time step  $t_n$  are calculated based on their values at time step  $t_{n-1}$ . Concerning the model, the signal data is stored each time step, to be called up in the next time step. This means that the valve responds based on the pressure in the grid and position of the valve at time step  $t_{n-1}$ , while the position of the valve at  $t_{n-1}$  is calculated for the pressure in the grid at  $t_{n-2}$ . This would mean that the valve would overfill the gas grid. The anomalies that rise from this are dealt with by adding the buffer flow described in paragraph 3.2.3.2 to the model.

### 5.3.2 Model behaviour

As can be seen in Figure 4.4.1, there is a discrepancy between the daily peak pressures in the historical data and the ones obtained from the model. While no clear evidence has been found on why this is the case, there are two reasons that might explain why this discrepancy occurs. The first reason is visible in Figure 4.5.1; the pressure in the grid lies about 0,1 bar above the lower limit of 4,5 bar. Although the deviation of 0,1 bar is a tolerated deviation, the grid at that time is being pumped up by the gas receiving station, while it does not have to be pumped up; this is also an effect of storing signal data from old time steps described in paragraph 5.3.1.

The second reason is visible in Figure 4.5.4; The modelled flow needs to stay within a 10% interval of the set point. Each time it leaves this interval when pressure is building up, the valve will be opened slightly and the new measured flow will be very close to the set point, but will not exceed it. When the old control algorithm had to intervene, it responded by closing the valve by more increments than the new control. This resulted in the flow through the valve being larger than the set point.

Combining both proposed reasons shows that over the course of the pressure in the grid building up, the old algorithm would let more gas flow through the valve, while it also operated with a higher initial pressure in the grid.



### 5.3.3 Model anomalies

There are some anomalies in pressure measured in the model. This has to do with data flaws in the 2013 data used to design some parameters. As can be seen in Figure 4.4.1, the pressure in the grid falls below 4,5 bar around time step  $0,7(x10^6)$ . This is due to an anomaly in the calculated gas consumption in the grid, as can be seen in Figure F.2 in Appendix F. This anomaly is caused by a sudden drop in pressure difference caused by the closing of one of the butterfly valves in Figure 2.3.1 in order to reduce noise pollution from the system. This is also the cause for the others anomalies in gas consumption in Figure F.2 that lie close to this point. The anomaly on time step  $2,3(x10^6)$  is caused by an error in the system, which had it sending out the same values for all parameters for four hours, while the actual values of the parameters in the system differed from these values. This resulted in the peak flow seen in Figure 4.4.4 at this time step.

At five time steps during the simulation, the set point could not be reached since the pressure difference was zero. During these moments, the flow through the valve varies a lot as it tries to reach the set point. Nevertheless, the old algorithm appears to perform better than the new control. The reason for this is that the new control is designed to respond faster to changing conditions, which means that its response action is larger than that of the old control algorithm. This causes in the grid filling up more quickly, leading to a new time step with (almost) no pressure difference across the valve.

## 6 Conclusion

In order to solve the instability of the constant flow control, the main question of this research is whether it can be assured that the flow of gas from the constant flow rate controller remains equal to the set point under all circumstances. In order to answer this main research question, answers to the formulated sub-questions are provided first.

The characteristic of the valve is shown in Figure 4.2.1, corresponds with valve characteristics obtained from theory and is calculated using equation ( 10 ). The operational range of the valve is found to be  $66^\circ$  with a dead valve stroke of  $12^\circ$  and a free valve stroke of  $78^\circ$ . In the new control algorithm, the ideal position of the valve in the flow regulator is determined based on the following input signals: set point  $Q_{sn}$ , pressure difference across the valve  $\Delta p$ , pressure in the grid  $p_0$  and temperature of the gas  $T$ . The pressure loss in the SG3 system is found to be negligible with a loss of just  $4,4 \cdot 10^{-2}$  bar and the flow does not choke in the system. The system constraints therefore do not restrict dynamic behaviour of the constant flow rate control.

The new control concept has been tested in a model and in a field test to show whether it is able to cope with the changing circumstances that have occurred in the 2013 test. The new control concept is able to sustain a constant flow within 10% of the set point in both the model as well as the field test. The new valve control also shows to develop less pressure peaks, which means that there is more capacity for Green Gas in the grid. Thirdly, the new valve control algorithm can keep a more constant pressure in the grid.

Regarding the response to adapting conditions, the new valve control responds more quickly to a change in conditions than the old control and just as important, it does respond without skipping of the 10% interval over the set point.

Overall, it appears that the developed constant flow algorithm can assure that the flow of gas from the constant flow rate controller remains equal to the set point under all circumstances. Both the model and the field test show positive results and all that rests for the new algorithm is to prove itself during the demonstration project.

### 6.1 Recommendations

Over the course of this research, and also from the 2012 and 2013 field test, it became apparent that some hardware in the SG3 system is not designed for this particular application. For new tests, it is best to further develop the SG3 system. Two parts that should be replaced are the ball valve and the gas meter. A ball valve is not designed for constant flow control under varying pressure, so other options should at least be explored.

Another flaw in the current SG3 system is the gas meter that is used to measure the flow through the system. The time between bona fide measurements of the flow is too large for the system to apply constant flow control on, especially for small flows (smaller than  $500 \text{ Nm}^3/\text{h}$ ). This could be tackled by replacing the gas meter with a mass flow meter.

These redevelopments of the SG3 system should mitigate most start-up problems that occur in a new system like this. What is most important for the future of the SG3 system, is the long term applications that distribution system operators see for this particular system. The current most likely application, where the system is effectively placed between the gas receiving station and the gas grid, entails that the system should match the reliability of the gas receiving station. At the same time, the major uncertainty of the new control algorithm is its reliability over a longer period of time. This will become clear during the 2016 demonstration of dynamic gas grid management.

## 7 References

- Beurskens, L. W. M., Hekkenberg, M., & Vethman, P. (2011). Renewable energy projections as published in the national renewable energy action plans of the European member states. *European Research Centre of the Netherlands (ECN) and European Environmental Agency (EEA), Petten*.
- Chern, M. J., Wang, C. C., & Ma, C. H. (2007). Performance test and flow visualization of ball valve. *Experimental thermal and fluid science*, 31(6), 505-512.
- Edmister, W. C., & Lee, B.I. (1984). Applied hydrocarbon thermodynamics. Volume 1. *Houston, Gulf Publishing Company*.
- Geerssen, T. M. (1988). Physical properties of natural gases. *NV Nederlandse Gasunie*.
- Holman, J. P. (2001). Heat transfer, Eighth SI Metric Edition.
- Kast, W., & Nirschl, H. (2013). VDI-Wärmeatlas Section L1.3. (11. Auflage) *Springer-Verlag, Berlin Heidelberg*.
- Katz, D. L. V., Cornell, D., Kobayashi, R., Poetmann, F. H., Vary, J. A., Elenbaas, J. R., Weinaug, C. F. (1959). Handbook of natural gas engineering. New York, McGraw-Hill Book Company.
- Techo, R., Tickner, R. R., & James, R. E. (1965). An accurate equation for the computation of the friction factor for smooth pipes from the Reynolds number. *Journal of Applied Mechanics*, 32(2), 443-443.

# Appendix

## A. Friction coefficient characteristics

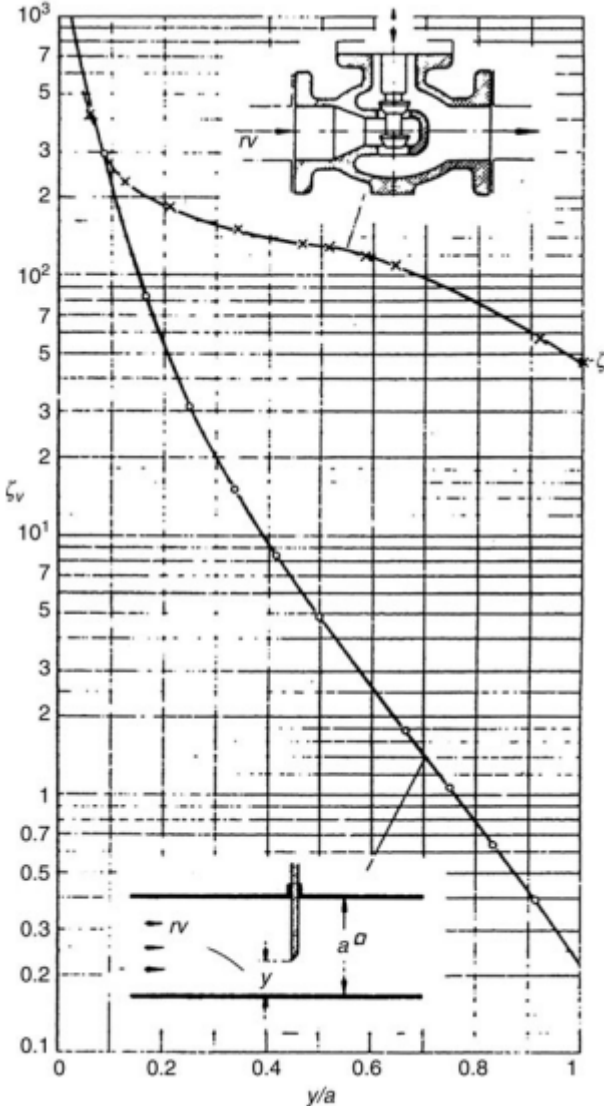


Figure A.1 - friction coefficient characteristic curve of a slider, lower line (Kast & Nirschl, 2013)

## B. SG3 system



Figure B.1 - the current SG3 system at gas receiving station Baarn

### C. Dynamic viscosity

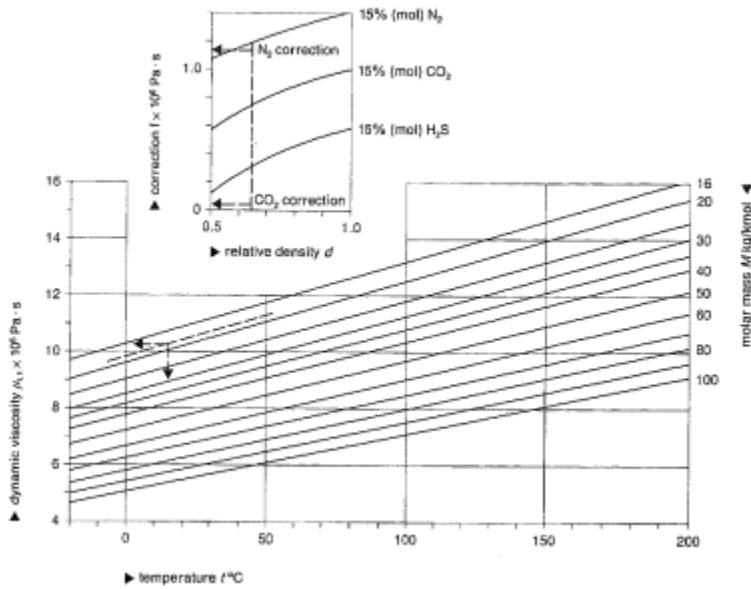


Figure C.1 - Dynamic viscosity  $\mu_{t,1}$  for gases as a function of temperature  $t$  and Molar mass  $M$  with a correction factor for the presence of  $\text{N}_2$ ,  $\text{CO}_2$  and  $\text{H}_2\text{S}$  inserted (Geerssen, 1988)

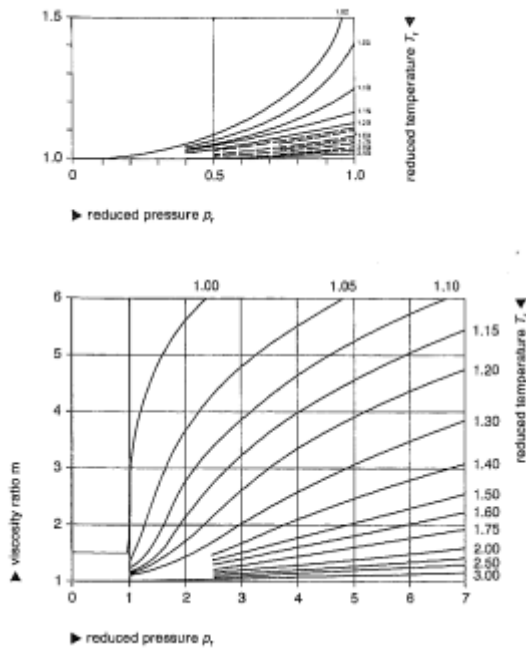


Figure C.2 - Viscosity ratio  $m$  as a function of reduced pressure  $p_r$  and reduced temperature  $T_r$  (Geerssen, 1988)

## D. Pressure loss in the system

### D1. Straight pipes

In order to calculate the pressure loss per straight pipe segment, friction coefficient  $\zeta$  from equation ( 29 ) is expressed as:

$$\zeta = \lambda \frac{l}{d} \quad ( 33 )$$

In which  $l$  is the length of the pipe in meters,  $d$  is the diameter of the pipe in meters and  $\lambda$  is the dimensionless friction factor, which depends on the type of flow (laminar or turbulent). When the Reynolds number is smaller than 2300, a flow is laminar. When it is larger than 4000, the flow is turbulent. When the Reynolds number is between 2300 and 4000, the flow is in transition (the flow is neither laminar nor turbulent) (Holman, 2001). For laminar flows, the friction factor is acquired from:

$$\lambda = \frac{64}{Re} \quad ( 34 )$$

For turbulent (and transition) flows, the method of obtaining the friction factor depends on the roughness of the pipe. The dimensionless relative surface roughness  $\varepsilon$  of piping is defined as:

$$\varepsilon = \frac{K}{d} \quad ( 35 )$$

where  $K$  is the average height of the protrusions in the pipe in meters, and  $d$  is the diameter of the pipe in meters. The average height of protrusions in the pipe depends on the material of the pipe. Turbulent flows through a pipe with relative roughness smaller than  $1 \cdot 10^{-5}$  are considered to be 'smooth', while turbulent flows through pipes with relative roughness larger than  $1 \cdot 10^{-5}$  are considered to be 'rough'. For smooth pipes, the friction factor is calculated through:

$$\lambda = \frac{0,3164}{\sqrt[4]{Re}} \quad ( 36 )$$

which holds for turbulent flows with a Reynolds number smaller than  $10^5$ . For rough turbulent flows, the friction factor is calculated through the following formula by Techo et al. (1965):

$$\lambda = \left[ -0,8685 \ln \left( \frac{1,964 \ln(Re) - 3,8215}{Re} + \frac{K}{3,71 * d} \right) \right]^{-2} \quad ( 37 )$$

### D2. Bended pipes

For laminar flows through bended pipes, dimensionless friction factor  $\lambda_b$  is calculated through:

$$\lambda_b = \lambda \left( 1 + 0,033 \left[ \log \left( Re \sqrt{\frac{d}{D}} \right) \right]^4 \right) \quad ( 38 )$$

which is valid for  $1 < Re \sqrt{\frac{d}{D}} < Re_c \sqrt{\frac{d}{D}}$ , for which  $Re_c$  is obtained from:

$$Re_c = 2300 \left( 1 + 8,6 \left[ \frac{d}{D} \right]^{0,45} \right) \quad ( 39 )$$

where  $d$  is the diameter of the pipe in meters and  $D$  is the average diameter of the coil in meters. This is obtained from:

$$D = \frac{2\pi l}{\theta \pi} \quad (40)$$

in which,  $l$  is the length of the pipe segment in meters and  $\theta$  is the angle between the two branching pieces of piping.

For turbulent flow through bended pipes, friction factor  $\lambda_b$  is calculated through:

$$\lambda_b = \lambda \left( 1 + 0,095 \left[ \frac{d}{D} \right]^{0,5} * Re^{0,25} \right) \quad (41)$$

which is valid for  $Re_c < Re < 1 \times 10^5$ . Both formulas are not valid for short bends and for s-shaped bends, where the distance between the bends is less than the diameter of the pipe. In order to calculate the friction coefficient per bended segment, equation ( 33 ) is rewritten as:

$$\zeta = \lambda_b \frac{l}{d} \quad (42)$$

### D3. Gradual expanding segments

For gradual expanding pipe segments applies that additional friction occurs in the pipe. The additional friction that occurs in these pipe segments is calculated through:

$$\zeta = \zeta_e \left( 1 - \frac{A_1}{A_2} \right)^2 \quad (43)$$

where  $A_1$  and  $A_2$  are cross-sectional areas in the pipe calculated with equation ( 15 ) and  $\zeta_e$  is the dimensionless resistance coefficient. This dimensionless resistance coefficient  $\zeta$  is a function of angle  $\alpha$  and the ratio  $\frac{d_2}{d_1}$ . Angle  $\alpha$  is shown in Figure D.1 and is calculated through:

$$\alpha = 2 \tan \left( \frac{\frac{1}{2}(d_2 - d_1)}{l} \right) \quad (44)$$

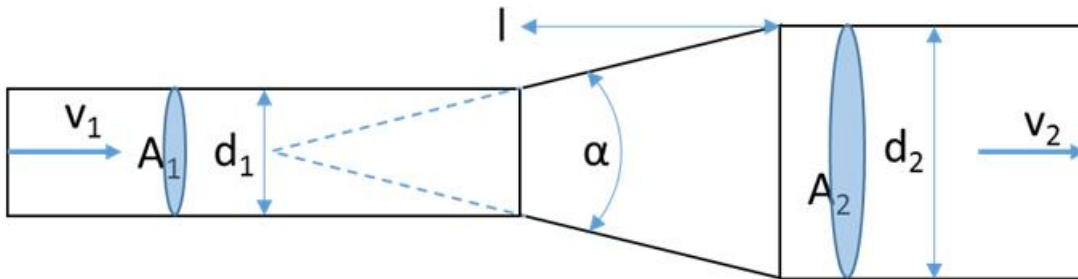


Figure D.1 - gradual enlargement in pipes

### D4. Gradual contracting segments

For gradual contracting flows, the pressure losses are very small when the contraction angle  $\beta$  in Figure D.2 is less than  $40^\circ$ . Angle  $\beta$  can be calculated through:



$$\beta = 2 \tan \left( \frac{1}{2} \frac{(d_1 - d_2)}{l} \right) \quad (45)$$

The friction coefficient for gradual contracting flows is then given as 0,04 (Kast & Nirschl, 2013).

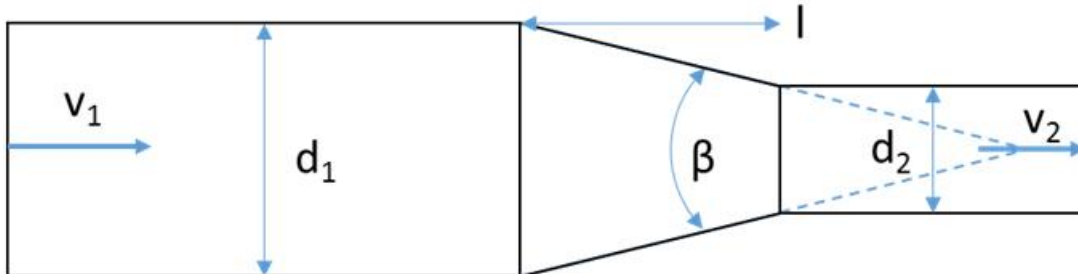


Figure D.2 - gradual contraction in pipes

#### D5. Tee fittings

The tee fittings present in the SG3 system can be seen as straight angled non-curved bends. The dimensionless friction coefficient is then a function of ratios  $\frac{Q_1}{Q_2}$  and  $\frac{A_2}{A_1}$ , and angle  $\theta$ , which is the angle between the two branching pieces of piping. This relation is shown in Figure D.3 in and is also applied for flow from a tee with a blindsided flange.

#### D6. Butterfly valves

For calculating the pressure loss through butterfly valves, the dimensionless friction coefficient is a function of ratio  $\frac{\varphi_0 - \varphi}{\varphi_0}$  where angle  $\varphi_0$  is the angle between the fully opened position of the valve and the fully closed position of the valve, while  $\varphi$  is the angle between the fully opened position of the valve and the position of the valve. This relation is shown in Figure D.4.

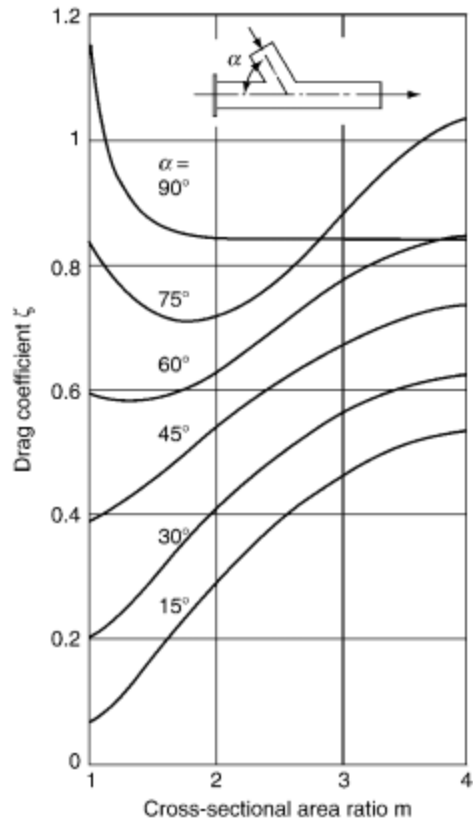


Figure D.3 - Friction coefficient  $\zeta$  for flow into a tee with a blind flange on the one branch (Kast & Nirschl, 2013)

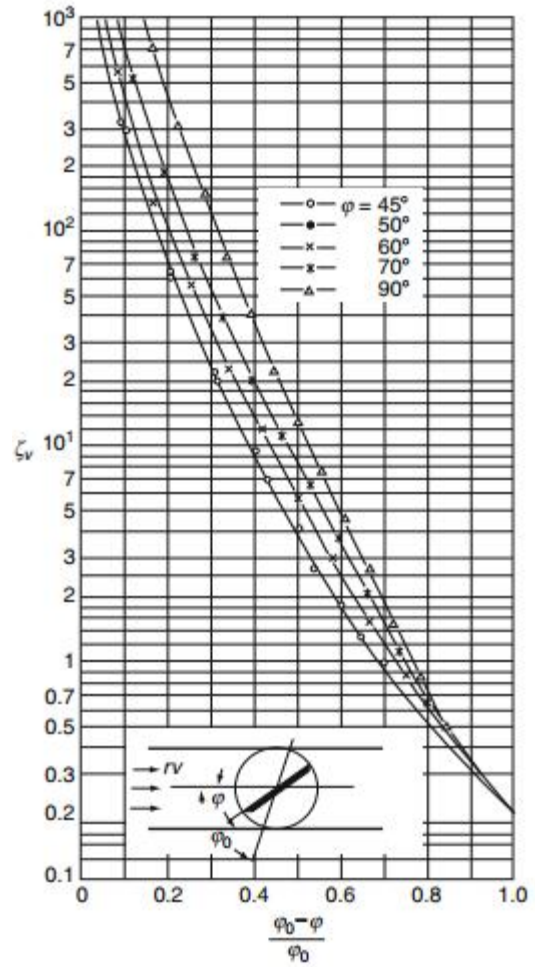


Figure D.4 - characteristic for a butterfly valve (Kast & Nirschl, 2013)

## E. Critical pressure ratio

### E1. Isobaric heat capacity

Specific isobaric heat capacity  $c_p$  is given by:

$$c_p = c_p^0 + \Delta c_p \quad (46)$$

where  $c_p^0$  is the ideal component, which depends on the temperature of the gas in the grid, and  $\Delta c_p$  is the real component, which is calculated through:

$$\Delta c_p = \Delta c_p^0 + \omega * \Delta c_p' \quad (47)$$

where  $\omega$  is the dimensionless acentric factor, which for Dutch natural gas is 0,0209 (Geerssen, 1988). Components  $\Delta c_p^0$  and  $\Delta c_p'$  are a function of reduced pressure  $p_r$  and reduced temperature  $T_r$ , which are obtained using equations ( 27 ) and ( 28 ).

In Figure E.1 can be found that  $\Delta c_p^0$  is 1,16 kJ/(kmol\*K) and in Figure E.2 can be found that  $\Delta c_p'$  is 1,03 kJ/(kmol\*K) for reduced pressure 0,202 and reduced temperature 1,514. This means that  $\Delta c_p$  is found to be 1,18 kJ/(kmol\*K) through equation ( 47 ). Ideal component  $c_p^0$  at 283,15 K is obtained from Table E.2, where the values at 283,15 K have been obtained through linear interpolation. The value of  $c_p^0$  is 35,272 kJ/(kmol\*K) which means that isobaric heat capacity  $c_p$  is 36,45 kJ/(kmol\*K) through equation ( 46 ).

### E2. Isochoric heat capacity

Isochoric heat capacity  $c_v$  in J/(mol\*K) is calculated through:

$$c_v = c_p - z * R_a \frac{\left[ 1 + \frac{T_0}{z} \left( \frac{\partial z}{\partial T} \right)_p \right]^2}{\left[ 1 - \frac{p}{z} \left( \frac{\partial z}{\partial p} \right)_T \right]} \quad (48)$$

which is rewritten as:

$$c_v = c_p - z * R_a \frac{N_2}{N_1} \quad (49)$$

$$N_1 = 1 - \frac{p}{z} \left( \frac{\partial z}{\partial p} \right)_T \quad (50)$$

$$N_2 = 1 + \frac{T_0}{z} \left( \frac{\partial z}{\partial T} \right)_p \quad (51)$$

where  $R_a$  is the universal gas constant of 8,31441 J/(mol\*K),  $p$  is the absolute pressure of the gas in kPa,  $T_0$  is the absolute temperature of the gas in kelvin and  $z$  is the dimensionless compressibility factor of the gas at  $p$  and  $T$ . Compressibility factor  $z$  and partial derivatives  $\left( \frac{\partial z}{\partial p} \right)_T$  and  $\left( \frac{\partial z}{\partial T} \right)_p$  are functions of absolute pressure and absolute temperature.

For  $N_1$ , the gradient of partial derivative  $\left( \frac{\partial z}{\partial p} \right)_T$  is calculated by dividing the absolute difference between  $z$  at  $T, p_n$  (0,9980) and  $z$  at  $T, p$  (0,9825) by the absolute difference between  $p_n$  (1,01325 bar) and  $p$  (9,01325 bar) at temperature  $T_0$  (283,15 K), which gives  $-1,938 * 10^{-5} \text{ bar}^{-1}$ .  $N_1$  is found to be 1,000 through equation ( 50 ) at absolute pressure  $p$ ,  $z$  at  $T, p$  and partial derivative  $\left( \frac{\partial z}{\partial p} \right)_T$ .

For N<sub>2</sub>, the gradient of partial derivative  $\left(\frac{\partial z}{\partial T}\right)_p$  is calculated by dividing the absolute difference between z at T<sub>n,p</sub> (0,9801) and z at T,p by the absolute difference between T<sub>n</sub> (273,15 K) and T<sub>0</sub> at pressure p of the gas in the grid, which gives 2,44\*10<sup>-4</sup> K<sup>-1</sup>. N<sub>2</sub> is found to be 1,070 through equation ( 51 ) at absolute temperature T, z at T,p and partial derivative  $\left(\frac{\partial z}{\partial T}\right)_p$ .

The isochoric heat capacity is calculated through equation ( 49 ) and is found to be 27,10 kJ/(kmol\*K) with c<sub>p</sub> of 36,45 kJ/(kmol\*K), compressibility factor z at T,p of 0,9825, R<sub>a</sub> of 8,31441 J/(mol\*K), N<sub>1</sub> of 1,000 and N<sub>2</sub> of 1,070.

### E3. Compressibility factor

Compressibility factor z is determined through the method of Edmister (Edmister & Lee, 1988), which uses the following equations:

$$z = z^0 + \frac{\omega}{\omega_r} (z^r - z^0) \quad (52)$$

$$z^{r,0} = V_r * \frac{p_r}{T_r} \quad (53)$$

$$V_r = \frac{T_r}{p_r} * \left( 1 + \frac{B}{V_r} + \frac{C}{V_r^2} + \frac{D}{V_r^5} + \frac{c_4}{T_r^3 * V_r^2} * \left( \beta + \frac{\gamma}{V_r^2} \right) e^{(-\gamma/V_r^2)} \right) \quad (54)$$

$$B = b_1 - \frac{b_2}{T_r} - \frac{b_3}{T_r^2} - \frac{b_4}{T_r^3} \quad (55)$$

$$C = c_1 - \frac{c_2}{T_r} + \frac{c_3}{T_r^3} \quad (56)$$

$$D = d_1 + \frac{d_2}{T_r} \quad (57)$$

with the following constants, shown in Table E.1:

Table E.1 - Constants for the compressibility factor (Geerssen, 1988)

	Simple fluid (z <sup>0</sup> )	Reference fluid (z <sup>r</sup> )
b <sub>1</sub>	0,1181193	0,0206579
b <sub>2</sub>	0,265728	0,331511
b <sub>3</sub>	0,154790	0,027655
b <sub>4</sub>	0,030323	0,203488
c <sub>1</sub>	0,0236744	0,0313385
c <sub>2</sub>	0,0186984	0,0503618
c <sub>3</sub>	0,0	0,016901
c <sub>4</sub>	0,042724	0,041577
d <sub>1</sub> *10 <sup>4</sup>	0,155488	0,48736
d <sub>2</sub> *10 <sup>4</sup>	0,623689	0,0740336
β	0,65392	1,226
γ	0,060167	0,03754

and variables reduced pressure p<sub>r</sub>, calculated through equation ( 27 ), reduced temperature T<sub>r</sub>, calculated through equation ( 28 ), acentric factor ω of natural gas of 0,0209 as well as reference acentric factor ω<sup>r</sup> of 0,3978 (Geerssen, 1988). This gives a compressibility factor z of 0,9825 at a pressure of 9,01325 bar and temperature of 283,15 K.

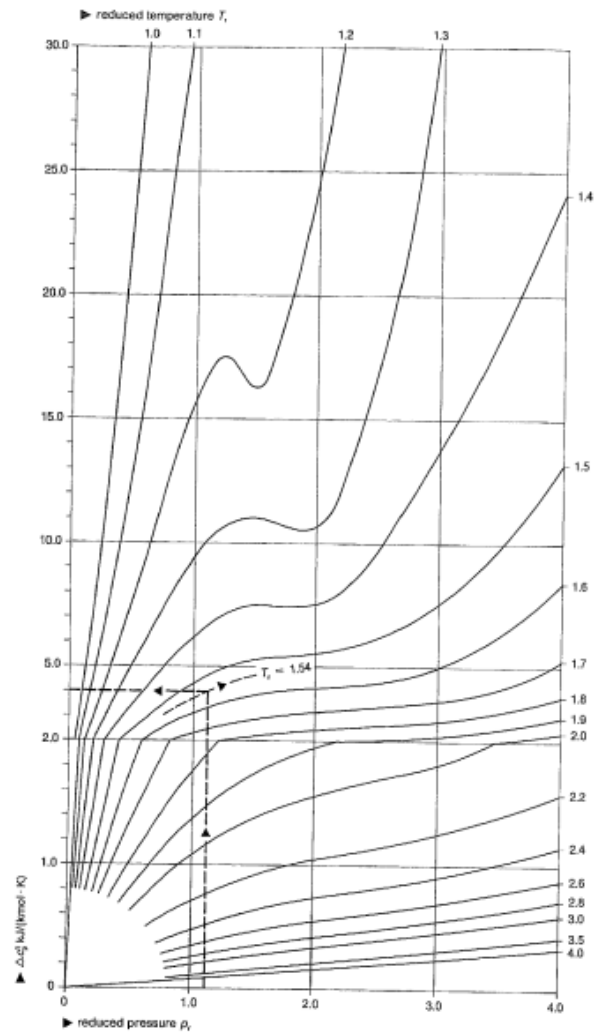
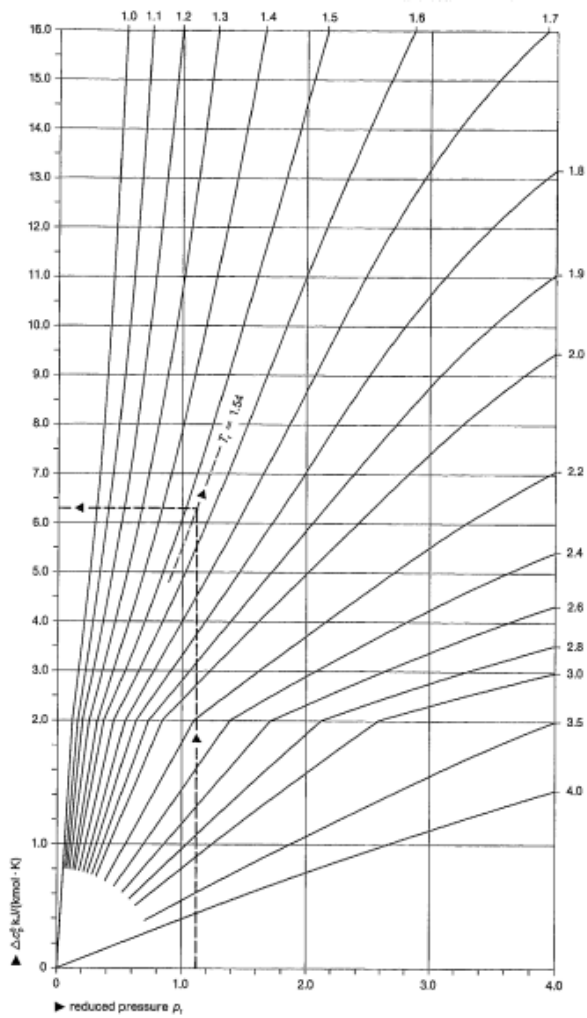


Figure E.1 -  $\Delta c_p^0$  as a function of reduced pressure  $p_r$  and reduced temperature  $T_r$  (Geerssen, 1988)

Figure E.2 -  $\Delta c_p'$  as a function of reduced pressure  $p_r$  and reduced temperature  $T_r$  (Geerssen, 1988)

Table E.2 -  $c_p^0$  of Dutch natural gas

Component	Formula	N	$c_p$ at 273,15 K'	$c_p$ at 288,15 K'	$c_p$ at 283,15 K
		% mol	kJ/(kmol*K)	kJ/(kmol*K)	kJ/(kmol*K)
Methane	CH <sub>4</sub>	81,29	35,08	35,581	35,414
Ethane	C <sub>2</sub> H <sub>6</sub>	2,87	49,912	51,575	51,021
Propane	C <sub>3</sub> H <sub>8</sub>	0,38	69,257	72,02	71,099
Butane	C <sub>4</sub> H <sub>10</sub>	0,15	93,151	96,986	95,708
Pentane	C <sub>5</sub> H <sub>12</sub>	0,04	112,131	117,377	115,628
Hexane	C <sub>6</sub> H <sub>14</sub>	0,05	133,923	139,368	137,553
Nitrogen	N <sub>2</sub>	14,32	29,057	29,067	29,064
Oxygen	O <sub>2</sub>	0,01	29,172	29,25	29,224
Carbon dioxide	CO <sub>2</sub>	0,89	36,166	36,824	36,605
		100	34,949	35,433	35,272

' obtained from Geerssen, 1988

## F. Supporting graphs

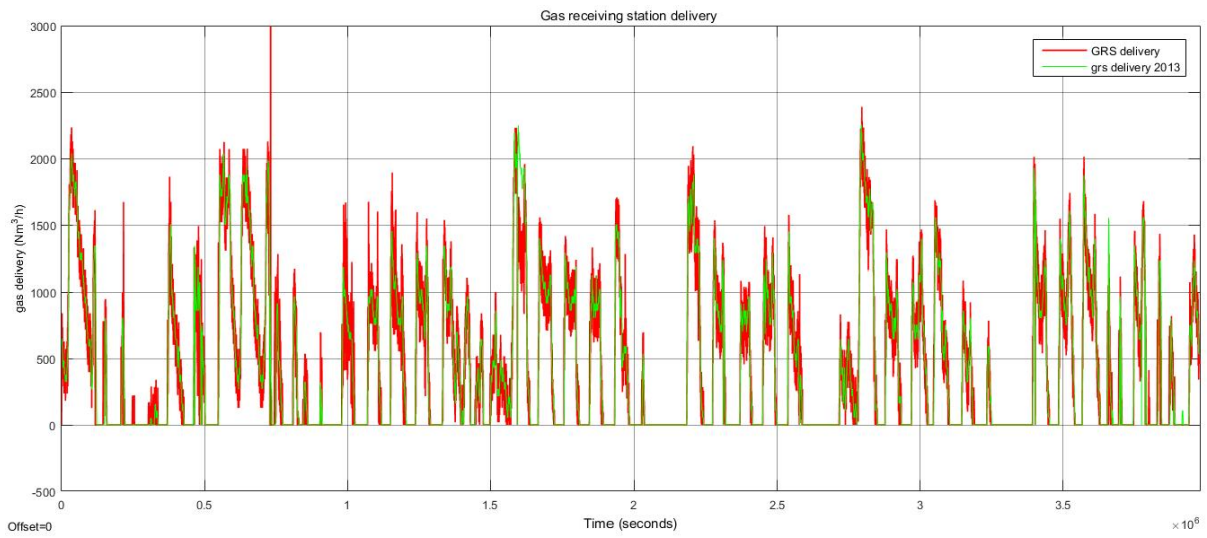


Figure F.1 - gas receiving station delivery, the peak at  $0,7 \times 10^6$  is due to the modelled gas receiving station correcting for missing data in the used dataset

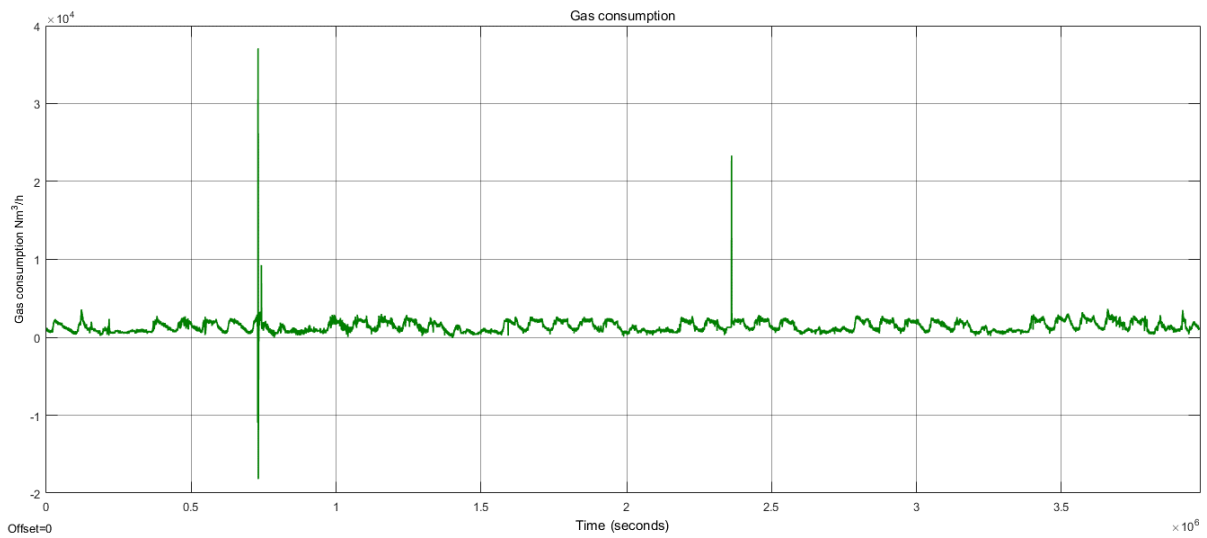


Figure F.2 - gas consumption in the model, peaks are due to noise reduction